

# The human proteome co-regulation map reveals functional relationships between proteins

Georg Kustatscher<sup>1\*</sup>, Piotr Grabowski<sup>2\*</sup>, Tina A. Schrader<sup>3</sup>, Josiah B. Passmore<sup>3</sup>, Michael Schrader<sup>3</sup>, Juri Rappsilber<sup>1,2#</sup>

<sup>1</sup> Wellcome Centre for Cell Biology, University of Edinburgh, Edinburgh EH9 3BF, UK

<sup>2</sup> Bioanalytics, Institute of Biotechnology, Technische Universität Berlin, 13355 Berlin, Germany

<sup>3</sup> Biosciences, University of Exeter, Exeter EX4 4QD, UK

\* Equal contribution

# Communicating author: juri.rappsilber@ed.ac.uk

Submission as *Resource* article.

The annotation of protein function is a longstanding challenge of cell biology that suffers from the sheer magnitude of the task. Here we present ProteomeHD, which documents the response of 10,323 human proteins to 294 biological perturbations, measured by isotope-labelling mass spectrometry. We reveal functional associations between human proteins using the treeClust machine learning algorithm, which we show to improve protein co-regulation analysis due to robust selectivity for close linear relationships. Our co-regulation map identifies a functional context for many uncharacterized proteins, including microproteins that are difficult to study with traditional methods. Co-regulation also captures relationships between proteins which do not physically interact or co-localize. For example, co-regulation of the peroxisomal membrane protein PEX11 $\beta$  with mitochondrial respiration factors led us to discover a novel organelle interface between peroxisomes and mitochondria in mammalian cells. The co-regulation map can be explored at [www.proteomeHD.net](http://www.proteomeHD.net).

Functional genomics approaches often use a “guilt-by-association” strategy to determine the biological function of genes and proteins on a system-wide scale. For example, high-throughput measurement of protein-protein interactions<sup>1–5</sup> and subcellular localization<sup>6–9</sup> has delivered invaluable insights into proteome organisation. A limitation of these techniques is that extensive biochemical procedures and cross-reacting antibodies may introduce artifacts. Moreover, not all proteins that function in the same biological process also interact physically or co-localize. Such functional relationships may be uncovered by assays with phenotypic readouts, including genetic interactions<sup>10</sup> and metabolic profiles<sup>11</sup>, but these have yet to be applied on a genomic scale in humans. One of the oldest functional genomics methods is gene expression profiling<sup>12</sup>. Genes with correlated activity often participate in similar cellular functions, which can be exploited to infer the function of uncharacterized genes based on their coexpression with known genes<sup>13–18</sup>.

However, predicting gene function from coexpression alone often leads to inaccurate results<sup>19,20</sup>. One possible reason for this is that gene activity is generally measured at the

39 mRNA level, neglecting the contribution of protein synthesis and degradation to gene  
40 expression control. The precise extent to which protein levels depend on mRNA abundances  
41 is still debated, and likely differs between genes and test systems<sup>21–23</sup>. However, some  
42 fundamental differences between mRNA and protein expression control have recently  
43 emerged. For example, many genes have coexpressed mRNAs due to their chromosomal  
44 proximity rather than any functional similarity<sup>19,24–26</sup>. Such non-functional mRNA coexpression  
45 results from stochastic transitions between active and inactive chromatin that affect wide  
46 genomic loci<sup>24,25,27</sup>, and transcriptional interference between closeby genes<sup>25,28</sup>. Importantly,  
47 coexpression of spatially close, but functionally unrelated genes is buffered at the protein  
48 level<sup>19,25</sup>. Protein abundances are also less affected than mRNA levels by genetic  
49 variation<sup>29,30</sup>, including variations in gene copy numbers<sup>31–33</sup>. Consequently, protein  
50 expression profiling outperforms mRNA expression profiling with regard to gene function  
51 prediction<sup>19,20</sup>. Protein-based profiling not only allows for a more accurate measurement of  
52 gene activity, but can determine additional aspects of a cell's response to a perturbation,  
53 such as changes in protein localization and modification state. At the proteome level,  
54 expression profiling can therefore be extended to a more comprehensive protein covariation  
55 analysis.

56 Proof-of-principle studies by us and others have shown that protein covariation can  
57 be used to infer, for example, the composition of protein complexes and organelles<sup>34–42</sup>.  
58 However, these studies have focussed on relatively small sets of proteins or biological  
59 conditions, or used samples tailored to the analysis of specific cellular structures. In addition  
60 to the limited amount of data, coexpression analyses may be held back by the statistical  
61 tools used to pinpoint genes with similar activity. Coexpressed genes are commonly  
62 identified using Pearson's correlation, which is restricted to linear correlations and  
63 susceptible to outliers. Machine-learning may offer an increase in sensitivity and specificity.

64 Despite the success of functional genomics, many human proteins remain  
65 uncharacterized, especially small proteins that are difficult to study by biochemical methods.  
66 The emergence of big proteomics data and new computational approaches could provide an  
67 opportunity to look at these proteins from a different angle. We wondered if protein  
68 covariation would assign functions to previously uncharacterized proteins or novel roles to  
69 characterized ones. The resulting resource is available at [www.proteomeHD.net](http://www.proteomeHD.net) to generate  
70 hypotheses on the cellular functions of proteins of interest in a straightforward manner.

## 71 RESULTS

### 72 ProteomeHD is a data matrix for functional proteomics

73 To turn protein covariation analysis into a system-wide, generally applicable method, we  
74 created ProteomeHD. In contrast to previous drafts of the human proteome<sup>8,9,22,43,44</sup>,  
75 ProteomeHD does not catalogue the proteome of specific tissues or subcellular  
76 compartments. Instead, ProteomeHD catalogues the transitions between different proteome  
77 states, i.e. changes in protein abundance or localization resulting from cellular perturbations.  
78 HD, or high-definition, refers to two aspects of the dataset. First, all experiments are  
79 quantified using SILAC (stable isotope labelling by amino acids in cell culture)<sup>45</sup>. SILAC

80 essentially eliminates sample processing artifacts and is especially accurate when  
81 quantifying small fold-changes. This is crucial to detect subtle, system-wide effects of a  
82 perturbation on the protein network. Second, HD refers to the number of observations  
83 (pixels) available for each protein. As more perturbations are analysed, regulatory patterns  
84 become more refined and can be detected more accurately.

85 To assemble ProteomeHD we processed the raw data from 5,288 individual  
86 mass-spectrometry runs into one coherent data matrix, which covers 10,323 proteins (from  
87 9,987 genes) and 294 biological conditions (Supplementary Table 1). About 20% of the  
88 experiments were performed in our laboratory and the remaining data were collected from  
89 the Proteomics Identifications (PRIDE)<sup>46</sup> repository (Fig. 1a). The data cover a wide array of  
90 quantitative proteomics experiments, such as perturbations with drugs and growth factors,  
91 genetic perturbations, cell differentiation studies and comparisons of cancer cell lines  
92 (Supplementary Table 2). All experiments are comparative studies using SILAC<sup>45</sup>, i.e. they  
93 do not report absolute protein concentrations but highly accurate fold-changes in response to  
94 perturbation. About 60% of the included experiments analysed whole-cell samples. The  
95 remaining measurements were performed on samples that had been fractionated after  
96 perturbation, e.g. to enrich for chromatin-based or secreted proteins. This allows for the  
97 detection of low-abundance proteins that may not be detected in whole-cell lysates.

### 98 **ProteomeHD offers high protein coverage**

99 On average, the 10,323 human proteins in ProteomeHD were quantified on the basis of 28.4  
100 peptides and a sequence coverage of 49% (Supplementary Fig. 1). As expected from  
101 shotgun proteomics data, not every protein is quantified in every condition. The 294 input  
102 experiments quantify 3,928 proteins on average. Each protein is quantified, on average, in  
103 112 biological conditions (Supplementary Fig. 1). As a rule of thumb, coexpression studies  
104 discard transcripts detected in less than half of the samples. However, with 294 conditions  
105 ProteomeHD is considerably larger than the typical coexpression analysis. We therefore  
106 decided to use a lower arbitrary cut-off and include proteins for downstream analysis if they  
107 were quantified in about a third of the conditions. Specifically, we focus our co-regulation  
108 analysis on the 5,013 proteins that were quantified in at least 95 of the 294 perturbation  
109 experiments. On average, these 5,013 proteins were quantified in 190 conditions; 43% were  
110 quantified in more than 200 conditions (Supplementary Fig. 1).

### 111 **Machine-learning captures functional protein associations**

112 Proteins that are functioning together have similar patterns of up- and down regulation  
113 across the many conditions and samples in ProteomeHD. For example, the patterns of  
114 proteins belonging to two well-known biological processes, oxidative phosphorylation and  
115 rRNA processing, can be clearly distinguished, even though most expression changes are  
116 well below 2-fold (Fig. 1b). Therefore, we reasoned that it should be possible to reveal  
117 functional links between proteins on the basis of such regulatory patterns, and reveal the  
118 function of unknown proteins by associating them with well-characterized ones.

119 Traditionally, the extent of coexpression between two genes is determined by  
120 correlation analysis, for example using Pearson's correlation coefficient (PCC). Since PCC is  
121 very sensitive to outlier measurements, Spearman's rank correlation ( $\rho$ ) or Biweight

122 midcorrelation (bicor) are sometimes used as more robust alternatives. We calculated these  
123 three correlation coefficients for all 12,562,578 pairwise combinations of the 5,013 protein  
124 subset of ProteomeHD. To assess which metric works best for ProteomeHD we performed a  
125 precision-recall analysis, using known functional protein - protein associations from  
126 Reactome<sup>47</sup> as gold standard. This showed no major difference between the correlation  
127 measures, although Spearman's rho performs slightly better than the others (Fig. 1c).

128 We then tested a new type of coexpression measure based on unsupervised  
129 machine-learning. Specifically, we used the treeClust algorithm developed by Buttrey and  
130 Whitaker, which infers dissimilarities based on decision trees<sup>48,49</sup>. In short, treeClust runs  
131 data through a set of decision trees, which it creates without explicitly provided training data,  
132 and essentially counts how often two proteins end up in the same leaves. This results in  
133 pairwise protein - protein dissimilarities (not clusters of proteins). Importantly, we find that  
134 treeClust dissimilarities strongly outperform the three correlation metrics at predicting  
135 functional relationships between proteins in ProteomeHD (Fig. 1c).

136 Finally, we apply a topological overlap measure (TOM)<sup>50,51</sup> to the treeClust  
137 similarities, which further enhances performance by approximately 10% as judged by the  
138 area under the precision-recall curve (Fig. 1c). The TOM is typically used to improve the  
139 robustness of correlation networks by re-weighting connections between two nodes  
140 according to how many shared neighbors they have. The TOM-optimised treeClust results  
141 form our "co-regulation score". This score is continuous and reflects how similar two proteins  
142 behave across ProteomeHD, i.e. the higher the score the more strongly co-regulated two  
143 proteins are. However, for some questions a simplified categorical interpretation is more  
144 straightforward. In these cases we arbitrarily consider the top-scoring 0.5% percent of  
145 proteins pairs as "co-regulated". In this way, we identify 62,812 co-regulated protein pairs  
146 (Fig. 1d, Supplementary Table 3). For comparison, if the same data were analysed by  
147 Pearson's correlation, selecting the top 0.5% pairs would correspond to a cut-off of PCC >  
148 0.69, which is generally considered a strong correlation.

149 We then tested whether co-regulation indicates co-function. Indeed, we find that  
150 co-regulated protein pairs are heavily enriched for subunits of the same protein complex,  
151 enzymes catalysing consecutive metabolic reactions and proteins occupying the same  
152 subcellular compartments (Fig. 1e). The majority of proteins are co-regulated with at least  
153 one other protein, and about a third have more than five co-regulation partners (Fig. 1f). For  
154 99% of the tested proteins that had  $\geq 10$  co-regulated pairs, the group of their co-regulation  
155 partners is enriched in at least one Gene Ontology<sup>52</sup> biological process (Fig. 1g).

### 156 **treeClust improves protein co-regulation analysis due to robust selectivity for close** 157 **linear relationships**

158 While decision trees are well-understood building blocks of many established  
159 machine-learning algorithms, treeClust itself is a relatively recent invention<sup>48</sup>. It was therefore  
160 unclear which type of information treeClust captures from a dataset. For example, treeClust  
161 scores could simply reflect whether or not two proteins are detected in the same set of  
162 samples, a measure that has been successfully exploited previously<sup>41</sup>. To test that we  
163 compared treeClust scores to the Jaccard index<sup>53</sup>, a dedicated measure of co-occurrence  
164 (Supplementary Fig. 2). In addition, we forced treeClust to learn dissimilarities solely based

165 on co-occurrence by using a “binary” version of ProteomeHD, where all SILAC ratios were  
166 turned into ones and all missing values into zeroes. We find that the Jaccard index and  
167 “binary” treeClust detect functionally related proteins equally well, but with much lower  
168 precision than standard treeClust. This suggests that protein co-regulation, i.e. coordinated  
169 changes in protein abundance, rather than co-detection is essential for treeClust  
170 performance.

171 Furthermore, it remained unclear what type of quantitative relationships treeClust can  
172 identify and why it outperforms correlation metrics for protein coexpression analysis. We  
173 address this by systematically benchmarking treeClust using synthetic data (reported in  
174 detail as a *Supplementary Note*). In short, we found that treeClust detects linear but not  
175 non-linear relationships. Unlike correlation metrics, it distinguishes between strong,  
176 tight-fitting relationships and weak trends. Finally, as may be expected from an algorithm  
177 based on decision trees, it is exceptionally robust against outliers. These properties of  
178 treeClust collectively explain its superior performance on ProteomeHD (*Supplementary*  
179 *Note*). However, experiments with synthetic data also show that treeClust works best for  
180 large datasets with 50 samples or more, depending on additional parameters such as the  
181 frequency of missing values. Traditional correlation analysis may be better suited for smaller  
182 gene expression datasets.

### 183 **A co-regulation map of the human proteome**

184 As a result of treeClust learning we know for each protein how strongly - or weakly - it is  
185 co-regulated with any other protein. In principle, these results could be displayed as a  
186 scale-free protein interaction network with edges indicating co-regulation (*Supplementary*  
187 *Fig. 3*). However, due to size and nature of our co-regulation data - 62,812 top-scoring links  
188 between 5,013 proteins - it appears impossible to avoid low-informative “hairball” graphs<sup>54</sup>.

189 We therefore chose to visualize the protein - protein co-regulation matrix using  
190 t-Distributed Stochastic Neighbor Embedding (t-SNE)<sup>55,56</sup>. This produces a two-dimensional  
191 proteome co-regulation map in which the distance between proteins indicates how similar  
192 they responded to the various perturbations in ProteomeHD (*Fig. 1h*, *Supplementary Table*  
193 *4*). Notably, t-SNE takes all pairwise co-regulation scores into account, rather than focussing  
194 on a small number of links above an arbitrary threshold. The t-SNE map shows that protein  
195 co-regulation is closely related to co-function. From a global perspective, the map reflects  
196 the subcellular organization of the cell (*Fig. 1i*). It broadly separates organelles and, for  
197 example, sets apart the nucleolus from the nucleus. A closer look into three sections of the  
198 map reveals that it captures more detailed functional relationships, too. For example, the five  
199 protein complexes of the respiratory chain are almost resolved (*Fig. 1i*, section 1). The  
200 section also contains the phosphate and ADP carriers that transport the substrates for ATP  
201 synthesis through the inner mitochondrial membrane, and ATP1F1 - a short-lived,  
202 post-transcriptionally controlled key driver of oxidative phosphorylation in mammals<sup>57</sup>.  
203 Similarly, cytoskeleton proteins such as actins and myosins are found next to their  
204 regulators, including Rho GTPases and the Arp2/3 complex (*Fig. 1i*, section 2). A third  
205 example section shows groups of proteins involved in RNA biology, from nucleolar rRNA  
206 processing to mRNA splicing and export (*Fig. 1i*, section 3). Notably, these annotations are  
207 only used to illustrate that the co-regulation map reflects functional similarity; the map itself is

208 generated without any curated information, solely on the basis of protein abundance  
209 changes in ProteomeHD. Therefore, the co-regulation map provides a data-driven overview  
210 of the proteome, connecting proteins into functionally related groups.

### 211 **Co-regulation complements existing functional genomics methods**

212 We next asked if protein co-regulation can predict associations that are not detected by other  
213 methods. For this we compare co-regulation to four alternative large-scale resources:  
214 IntAct<sup>58</sup>, BioGRID<sup>59</sup>, STRING<sup>60</sup> and BioPlex<sup>4</sup>. The first three are “meta-resources”, i.e. they  
215 compile curated sets of protein - protein interactions (PPIs) from the results of thousands of  
216 individual studies. Since meta-resources generally map interactions to gene loci rather than  
217 proteins, we disregard protein isoforms for this comparison and focus on co-regulated genes.

218 The co-regulation map covers fewer distinct genes than the other resources, but only  
219 STRING captures more interactions per average gene (Fig. 2a). Based on the 2,565 genes  
220 covered by both approaches, around 39% of the gene pairs identified as co-regulated had  
221 previously been linked in STRING (Fig. 2b). This suggests that co-regulation analysis  
222 confirms existing links, but also provides many additional ones. Conversely, only 7% of  
223 STRING PPIs are co-regulated, which may reflect the diverse molecular nature of  
224 associations covered by STRING. Notably, the overlap between the resources depends on  
225 the stringency setting: considering fewer, more stringent STRING interactions decreases the  
226 coverage of co-regulated genes and increases STRING PPIs identified as co-regulated (Fig.  
227 2b). An equivalent trend would be observed when modulating the co-regulation cut-off.  
228 STRING associations are based on multiple types of evidence, of which “mRNA  
229 coexpression” unsurprisingly shows the highest individual overlap with protein co-regulation  
230 results (Fig. 2c).

231 Next, we compared co-regulation specifically to physical PPIs catalogued by IntAct  
232 and BioGRID. We find that 11% of co-regulated gene pairs have a documented physical  
233 interaction between their proteins in BioGRID, and 3% are found in the smaller IntAct  
234 database (Fig. 2b). These physical PPIs were mainly derived from co-fractionation  
235 experiments, which tend to capture indirect interactions, rather than methods that detect  
236 direct interactions, such as two-hybrid screens (Fig. 2c).

237 Finally, we compared the co-regulation approach to an individual functional genomics  
238 project: BioPlex 2.0, the most comprehensive affinity purification–mass spectrometry  
239 (AP-MS) study reported to date<sup>4</sup>. BioPlex reports 4,935 physical interactions between the  
240 proteins used in our study, of which 19% are also co-regulated (Fig. 2d). An additional  
241 43,759 potential links between these proteins are identified uniquely by co-regulation. These  
242 are strongly enriched for functional protein associations found in STRING, compared to a  
243 random set of protein pairs (Fig. 2d). In conclusion, these comparisons suggest that protein  
244 co-regulation identifies protein - protein associations in a way that is reliable yet  
245 complementary to existing functional genomics methods. Note that proteins can interact  
246 physically or genetically or co-localize without being co-regulated, and vice versa. Therefore,  
247 protein co-regulation is complementary not just in terms of identifying new links, but also in  
248 providing additional, independent biological evidence for associations detected by other  
249 approaches.

## Uncharacterized proteins in ProteomeHD are rich in microproteins

The co-regulation map contains 301 uncharacterized proteins, which we define as proteins with a UniProt<sup>61</sup> annotation score of 3 or less (Fig. 2e). Of these, 51% are co-regulated with at least one fully characterized protein, i.e. a protein with an annotation score of 4 or 5 (Fig. 2f). On median, these uncharacterized proteins have 9 well-studied co-regulation partners, making it possible to predict their potential function in a “guilt by association” approach. We observe a similar connectivity for the cancer gene census<sup>62</sup>, i.e. genes that cause cancer when mutated, and for DisGeNET<sup>63</sup> genes, which are genes implicated in a broad range of human diseases (Fig. 2f). Therefore, protein co-regulation may also be helpful for functional analysis of human disease genes.

A common property of uncharacterized proteins is their small size. For example, proteins smaller than 15 kDa constitute 18% of the uncharacterized proteins in the human proteome, but only 5% of the characterized ones. Among the least well understood fraction of the proteome, i.e. proteins with an annotation score of 1, 40% are smaller than 15 kDa (Fig. 2g). This discrepancy is set to increase further, since hundreds or thousands such microproteins have so far been overlooked by genome annotation efforts<sup>64,65</sup>. Microproteins can regulate fundamental biological processes<sup>66</sup>, but their small size makes it difficult to identify interaction partners<sup>64,67</sup> or to target them in mutagenesis screens<sup>64</sup>. Microprotein sequences also tend to be less conserved than those of longer protein-coding genes<sup>68</sup>. We reasoned that our perturbation proteomics approach may help to reduce the annotation gap for small proteins. As it only requires proteins to be quantifiable in cell extracts we expect it to be less biased by protein size than methods involving extensive genetic or biochemical sample processing. Indeed, we find that 16% of the uncharacterized proteins in the co-regulation map are smaller than 15 kDa, which is close to the 18% in the proteome overall (Fig. 2h). However, it is a significant difference to BioPlex’s cutting-edge AP-MS data, in which microproteins drop to 6% ( $p < 2e-5$  in a one-tailed Fisher’s Exact test).

The fact that microproteins are not underrepresented in ProteomeHD does not automatically mean that their detection and characterisation is as robust as that of larger proteins. However, the average microprotein in the co-regulation map has been identified by 12.2 peptides, many of which overlap and together result in an average sequence coverage of 76.4% (Supplementary Fig. 4a, d). While in a typical SILAC experiment proteins are considered to be quantifiable from upwards of two independent observations (SILAC ratio counts), microproteins in the co-regulation map are quantified with an average of 9 ratio counts per experiment, totalling a median of 671 ratio counts across ProteomeHD (Supplementary Fig. 4b, c). This indicates that microprotein quantitation in ProteomeHD is robust. Surprisingly, we find that microproteins have more co-regulation partners than larger proteins, and the same is true for their connectivity in STRING (Supplementary Fig. 4f). Within STRING, the majority of microprotein interactions are derived from curated annotations rather than high-throughput efforts such as RNA coexpression and text mining (Supplementary Fig. 4g). Note that, based on BioGRID, microproteins engage in fewer physical PPIs than larger proteins. This may be the result of an experimental bias (microproteins may dissociate more easily during purification and are more difficult to detect) or reflect a biological property (microproteins may have fewer physical interaction partners).

293 In either case, co-regulation offers itself as a powerful alternative approach to study  
294 microprotein functions in a systematic way.

### 295 **Functional annotation of proteins by co-regulation**

296 To facilitate the characterization of proteins through co-regulation we created the website  
297 [www.proteomeHD.net](http://www.proteomeHD.net). It allows users to search for a protein of interest, showing its position  
298 in the co-regulation map together with any co-regulation partners (Supplementary Fig. 5).  
299 The online map is interactive and zoomable, making it easy to explore the neighborhood of a  
300 query protein. The co-regulation score cut-off can be adjusted and statistical enrichment of  
301 Gene Ontology<sup>52</sup> terms among the co-regulated proteins is automatically calculated.

302 For example, protein co-regulation can be used to predict the potential function of  
303 uncharacterized microproteins such as the mitochondrial proteolipid MP68. MP68 is  
304 co-regulated with subunits of the ATP synthase complex, suggesting a function in ATP  
305 production (Fig. 1i, section 1). Despite being only 6.8 kDa small, its presence in the  
306 co-regulation map is documented by 8 distinct peptides that were observed a total of 398  
307 times across 142 experiments (Supplementary Fig. 4e). Intriguingly, MP68 co-purifies  
308 biochemically with the ATP synthase complex, but only in buffers containing specific  
309 phospholipids<sup>69,70</sup>, and knockdown of MP68 decreases ATP synthesis in HeLa cells<sup>71</sup>.

310 Virtually nothing is known about the 12 kDa microprotein TMEM256, although  
311 sequence analysis suggests it may be a membrane protein. Its position in the co-regulation  
312 map (Fig. 2i) and GO analysis of its co-regulation partners indicates that it likely localizes to  
313 the inner mitochondrial membrane (GO:0005743, Bonferroni adj.  $p < 5e-40$ ), where it may  
314 participate in oxidative phosphorylation (GO:0006119,  $p < 3e-35$ ).

315 Some proteins have no co-regulation partners above the default score cut-off, but  
316 can still be functionally annotated through the co-regulation map. The uncharacterized 224  
317 kDa protein HEATR5B, for example, is located in an area related to vesicle biology (Fig. 2i).  
318 Its immediate neighbours are five subunits of the HOPS complex, which mediates the fusion  
319 of late endosome to lysosomes. The position in the map shows that the HOPS complex is  
320 the closest fit to HEATR5B's regulation pattern, but they are not as similar as the top-scoring  
321 pairs in our overall analysis. If the co-regulation score cut-off is lowered, HOPS subunits and  
322 other endolysosomal proteins are eventually identified as co-regulated with HEATR5B, with  
323 concomitant enrichment of the related GO terms. This suggests that HEATR5B may not itself  
324 be a HOPS subunit, but could have a related vesicle-based function. Notably, a biochemical  
325 fractionation profiling approach also predicted HEATR5B to be a vesicle protein<sup>72</sup>.

326 Multifunctional proteins appear to fall into two categories in terms of co-regulation  
327 behavior. Prohibitin, for example, functions both as a mitochondrial scaffold protein and a  
328 nuclear transcription factor<sup>73</sup>. However, only the mitochondrial function is represented in the  
329 co-regulation map (Fig. 2j). This could indicate that its nuclear activity is not relevant in the  
330 biological conditions covered by ProteomeHD, or that only a small intracellular pool of  
331 prohibitin is nuclear, so that changes in its nuclear abundance are insignificant in comparison  
332 to the mitochondrial pool. In contrast, the helicase DDX3X shuttles between nucleus and  
333 cytoplasm, functioning both as nuclear mRNA processing factor and cytoplasmic regulator of  
334 translation<sup>74</sup>. In the co-regulation map, DDX3X sits between the areas related to these two  
335 activities and is significantly co-regulated both with proteins involved in nuclear RNA biology



336 and with translation factors (Fig. 2j). Therefore, DDX3X is a multifunctional protein whose  
337 separate activities result in a mixed regulatory pattern.

338 The protein co-regulation data presented here have been integrated into the recently  
339 released 11th version of STRING<sup>75</sup> (<https://string-db.org/>). In STRING's human protein -  
340 protein association network, links between proteins inferred from co-regulation in  
341 ProteomeHD are shown as network edges of the "coexpression" type (Supplementary Fig.  
342 6). Therefore, STRING is an alternative source for users wishing to explore protein  
343 co-regulation in conjunction with other types of association evidence.

### 344 **A new function for PEX11 $\beta$ in peroxisome-mitochondria interplay**

345 Some well-characterized proteins have unexpected co-regulation partners. For example,  
346 PEX11 $\beta$  is a key regulator of peroxisomal membrane dynamics and division<sup>76</sup>. However,  
347 PEX11 $\beta$ 's co-regulation partners are not peroxisomal proteins but subunits of the  
348 mitochondrial ATP synthase and other components of the electron transport chain (Fig. 1i,  
349 section 1). These proteins are located to the inner mitochondrial membrane, making a  
350 physical interaction with PEX11 $\beta$  unlikely. However, peroxisomes and mitochondria in  
351 mammals are intimately linked cooperating in fatty acid  $\beta$ -oxidation and ROS homeostasis<sup>77</sup>.  
352 How these organelles communicate or mediate metabolite flux has been elusive. Live cell  
353 imaging revealed that expression of PEX11 $\beta$ -EGFP in mammalian cells induced the  
354 formation of peroxisomal membrane protrusions, which interact with mitochondria (Fig. 3,  
355 Supplementary movies 1-3). Interactions of elongated peroxisomes with mitochondria were  
356 more frequent than those of spherical organelles, but both interactions were long-lasting  
357 (Fig. 3n,o). This indicates that peroxisome elongation can facilitate organelle interaction, but  
358 once organelles are tethered, the duration of contacts is similar between different  
359 morphological forms. Miro1 (RHOT1), a membrane adaptor for the microtubule-dependent  
360 motors kinesin and dynein<sup>78</sup>, is also co-regulated with PEX11 $\beta$  (Fig. 1i, section 1). We and  
361 others recently showed that Miro1 distributes to mitochondria and peroxisomes<sup>79,80</sup> indicating  
362 that it coordinates mitochondrial and peroxisomal dynamics with local energy turnover.  
363 Peroxisome-targeted Miro1 (Myc-Miro-PO) can be used as a tool to exert pulling forces at  
364 peroxisomal membranes, which results in the formation of membrane protrusions in certain  
365 cell types<sup>81</sup> (Supplementary Fig. 7). We show here that silencing of PEX11 $\beta$  inhibits  
366 membrane elongation by Myc-Miro-PO, confirming that PEX11 $\beta$  is required for the formation  
367 of peroxisomal membrane protrusions (Supplementary Fig. 7). These findings are in  
368 agreement with studies in plants, where *At*PEX11a has been reported to mediate the  
369 formation of peroxisomal membrane extensions in response to ROS<sup>82</sup>. In yeast,  
370 peroxisome-mitochondria contact sites are established by ScPex11 and ScMdm34, a  
371 component of the ERMES complex<sup>83</sup>. Additional tethering functions for the yeast mitofusin  
372 Fzo1 and ScPex34 in peroxisome-mitochondria contacts have recently been revealed<sup>84</sup>.  
373 Importantly, the study also demonstrated a physiological role for peroxisome-mitochondria  
374 contact sites in linking peroxisomal  $\beta$ -oxidation and mitochondrial ATP generation by the  
375 citric acid cycle<sup>84</sup>. We conclude that PEX11 $\beta$  and Miro1 contribute to peroxisome membrane  
376 protrusions, which present a new mechanism of interaction between peroxisomes and  
377 mitochondria in mammals. They likely function in the metabolic cooperation and crosstalk  
378 between both organelles, and may facilitate transfer of metabolites such as acetyl-CoA

379 and/or ROS homeostasis during mitochondrial ATP production. These findings now enable  
380 future studies on the precise functions of peroxisome membrane protrusions in mammalian  
381 cells and the role of PEX11 $\beta$ .

### 382 **Proteomics enables higher accuracy but lower coverage than transcriptomics**

383 To compare the impact of mRNA and protein abundances on expression profiling we first  
384 focussed on 59 SILAC ratios in ProteomeHD that measured abundance changes across a  
385 panel of lymphoblastoid cell lines<sup>30</sup>. For these samples, corresponding mRNA abundance  
386 changes have been determined using RNA-sequencing<sup>85</sup>. Repeating treeClust learning on  
387 the basis of these data, we observed that protein coexpression predicts functional  
388 associations with far higher precision than mRNA coexpression (Fig. 4a). Similar results  
389 have recently been reported for a panel of human cancer samples<sup>19</sup>.

390 Such analyses show that in a direct gene-by-gene, sample-by-sample comparison,  
391 protein expression levels are better indicators for gene function than mRNA expression.  
392 However, the amount of transcriptomics data published to date vastly exceeds that of  
393 proteomics studies. For example, the NCBI GEO repository currently holds mRNA  
394 expression profiling data from more than one million human samples<sup>86</sup>. This raises the  
395 possibility that the sheer quantity of available transcriptomics data could overcome their  
396 reduced reflection of functional links and, in combined form, perform better than  
397 protein-based measurements. To test this we compared the ProteomeHD co-regulation  
398 score with Pearson correlation coefficients obtained by STRING, which leverages the vast  
399 amount of mRNA expression experiments deposited in GEO<sup>60,87</sup>. Remarkably,  
400 precision-recall analysis shows that the protein co-regulation score still outperforms mRNA  
401 coexpression, despite being based on only 294 SILAC ratios (Fig. 4b). Much of this  
402 improvement is due to the robustness of treeClust machine-learning, as Pearson's  
403 correlation coefficients derived from the same ProteomeHD data work only moderately better  
404 than mRNA correlation (Fig. 4b). While only gene pairs with both mRNA and protein  
405 expression measurements were considered for the precision-recall analysis, the  
406 transcriptomics and proteomics datasets individually covered 17,436 and 4,976 genes,  
407 respectively (Fig. 4b). Therefore, mRNA profiling outperforms protein profiling in terms of  
408 gene coverage. In addition, transcriptomics remains the only expression profiling approach  
409 suitable for non-coding RNAs.

## 410 **DISCUSSION**

411 ProteomeHD in conjunction with machine learning provides an entry point for "big-data"-type  
412 protein co-regulation analysis into the functional genomics methods repertoire. It is possible  
413 that accuracy and coverage could be increased further by adding additional proteomics data.  
414 To test this we randomly removed 5%, 10% or 15% of the data points in ProteomeHD. This  
415 decreases performance reproducibly and proportionally to the amount of removed data  
416 (Supplementary Fig. 8), suggesting that ProteomeHD has not reached saturation and  
417 expanding it will further enhance its performance. One possibility would be to incorporate  
418 other types of proteomics experiments, such as affinity-purifications or indeed the entire

419 PRIDE<sup>46</sup> repository. The latter approach is for instance taken by the Tabloid Proteome, which  
420 infers protein associations based on detecting them in the same subset of many different  
421 proteomics experiments<sup>41</sup>. However, there is a benefit of restricting ProteomeHD to  
422 perturbation experiments. It supports a biological interpretation of protein associations  
423 derived from it: two co-regulated proteins are part of the same cellular response to changing  
424 biological conditions, even though the precise molecular nature of the connection remains  
425 unknown. In this way, protein co-regulation analysis is analogous to genetic interaction  
426 screening. This also sets protein co-regulation apart from indiscriminate protein covariation  
427 or co-occurrence analyses, which find protein links in a mix of proteomics data and therefore  
428 give no insight into the possible biological connection.

429 A key difference between our approach and previous gene coexpression studies is  
430 our application of two machine-learning algorithms, treeClust<sup>48</sup> and t-SNE<sup>55,56</sup>. Inferring  
431 protein associations through treeClust learning is both more robust and sensitive than a  
432 traditional correlation-based approach, providing a leap in the accuracy with which  
433 functionally relevant interactions can be identified from the same dataset. For example, a  
434 recent study reported a protein co-regulation network across 41 cancer cell lines and  
435 subsequently identified dysregulated protein associations that predict drug sensitivities of  
436 these cell lines<sup>20</sup>. Applying Spearman's correlation to high-quality, TMT-based proteomics  
437 data allowed Lapek *et al*<sup>20</sup> to detect protein-protein associations with an accuracy that was  
438 tenfold higher than that based on matching mRNA coexpression data. When applying  
439 treeClust to these data, strikingly, we can further improve this performance (Supplementary  
440 Fig. 9a). This suggests that treeClust may be helpful for the detection of "dysregulation  
441 biomarkers" in the future. The second machine-learning tool we apply here, t-SNE, visualizes  
442 treeClust-learned protein associations as a 2D map. Correlation networks are typically built  
443 from a limited number of the strongest pairwise interactions, whereas t-SNE takes into  
444 account the similarity - or dissimilarity - between all possible pairwise protein combinations. It  
445 creates the map that best reflects both direct and indirect relationships between all proteins.  
446 In this way, also proteins that are not directly linked to the core network can be placed into a  
447 functional context. For example, a t-SNE co-regulation map obtained for Lapek *et al*'s cancer  
448 proteomics dataset contains the complete set of ~6,800 proteins, rather than the 3,024  
449 proteins that are directly correlated with another protein (Supplementary Fig. 9b). Moreover,  
450 protein-protein associations visualized by t-SNE can be explored in a hierarchical manner,  
451 with larger distances indicating weaker co-regulation. This may be useful for studying  
452 connections between related protein complexes (Fig. 1i) or to reveal broad functional clues  
453 for uncharacterized proteins for which no detailed predictions are available, such as the  
454 HEATR5B protein assigned to the vesicle area of the co-regulation map (Fig. 2i). Our web  
455 application at [www.proteomeHD.net](http://www.proteomeHD.net) is designed to support researchers in exploring  
456 co-regulation data at multiple scales, to validate existing hypotheses or create new ones.

457 Protein coexpression analysis identifies functional connections between proteins with  
458 an accuracy and sensitivity that is substantially higher than traditional mRNA coexpression  
459 analysis. This may be particularly important for constitutively active genes, which constitute  
460 about half of human genes<sup>44</sup> and are primarily controlled at the protein level<sup>88,89</sup>. With an ever  
461 increasing amount of protein expression data making their way into the public domain, and  
462 the simplicity of exploiting the analysis results by the scientific community, protein

463 coexpression analysis has a large potential for gene function annotation. Only 300  
464 quantitative proteomics measurements sufficed in conjunction with machine learning to  
465 establish functional connections between many human genes, which may be of considerable  
466 interest for proteome annotation in less studied or difficult to study organisms.

#### 467 **ACKNOWLEDGEMENTS**

468 We are grateful to Damian Szklarczyk for providing the mRNA Pearson correlation data used  
469 by STRING and the STRING team for testing our coregulation data and adding it as novel  
470 evidence type to STRING 11. We also thank Karen Wills, Kyosuke Nakamura, Constance  
471 Alabert and Anja Groth for contributing chromatin enrichment experiments, and Afsoon S.  
472 Azadi for support with live-cell-imaging. This work was supported by the Wellcome Trust  
473 through a Senior Research Fellowship to J.R. (grant number 103139) and by the  
474 Biotechnology and Biological Sciences Research Council (BB/N01541X/1, BB/R016844/1; to  
475 M.S.) and H2020-MSCA-ITN-2018 812968 PERICO (to M.S.). The Wellcome Centre for Cell  
476 Biology is supported by core funding from the Wellcome Trust (grant number 203149).

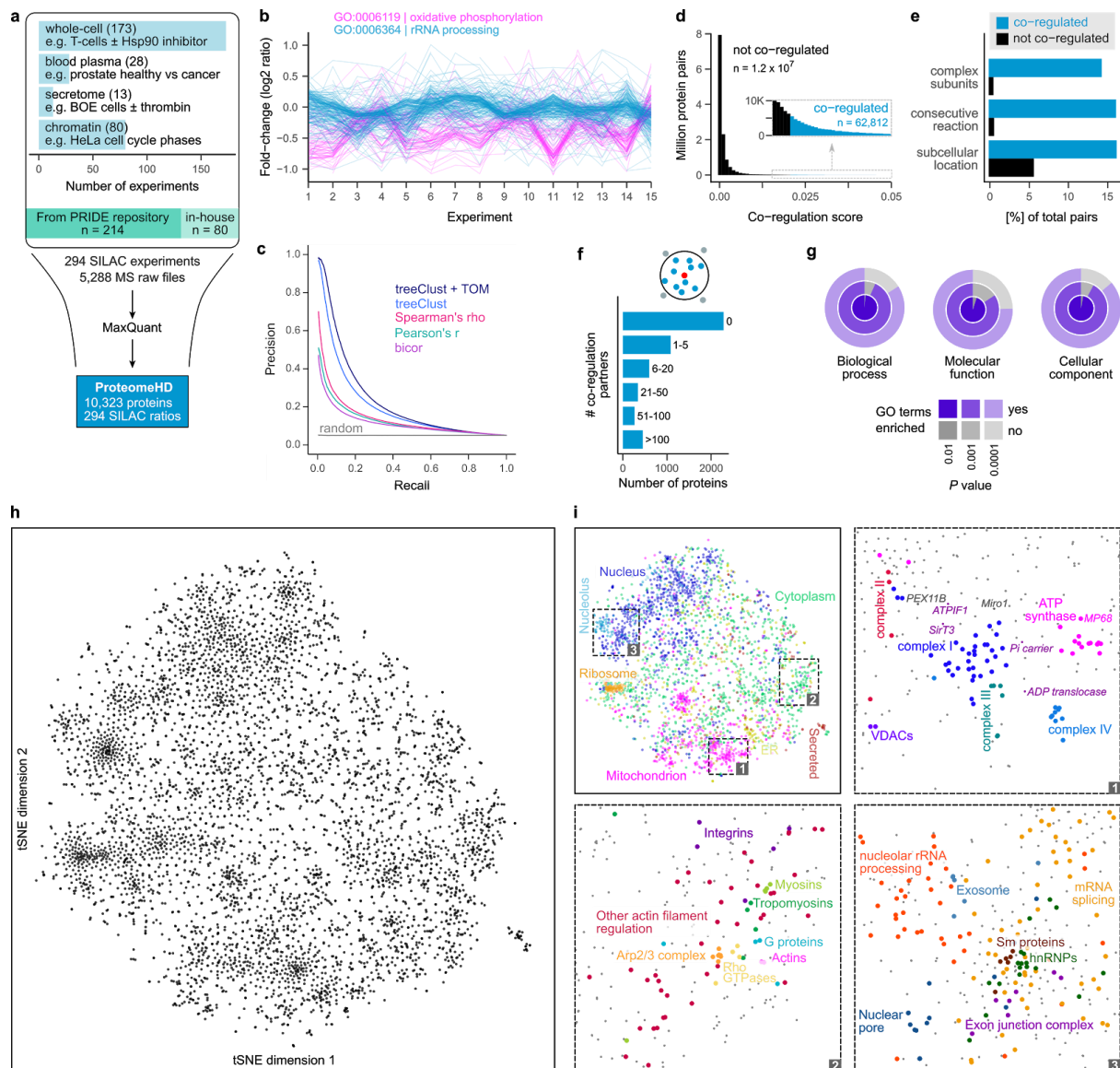
#### 477 **AUTHOR CONTRIBUTIONS**

478 G. K. and J. R. conceived the project. G. K. and P.G. conducted the data analysis. P. G.  
479 created the web application. T. A. S., J. B. P. and M. S. conducted the Pex11 $\beta$  analysis. All  
480 authors contributed to writing the manuscript.

#### 481 **COMPETING FINANCIAL INTERESTS**

482 The authors declare no competing financial interests.

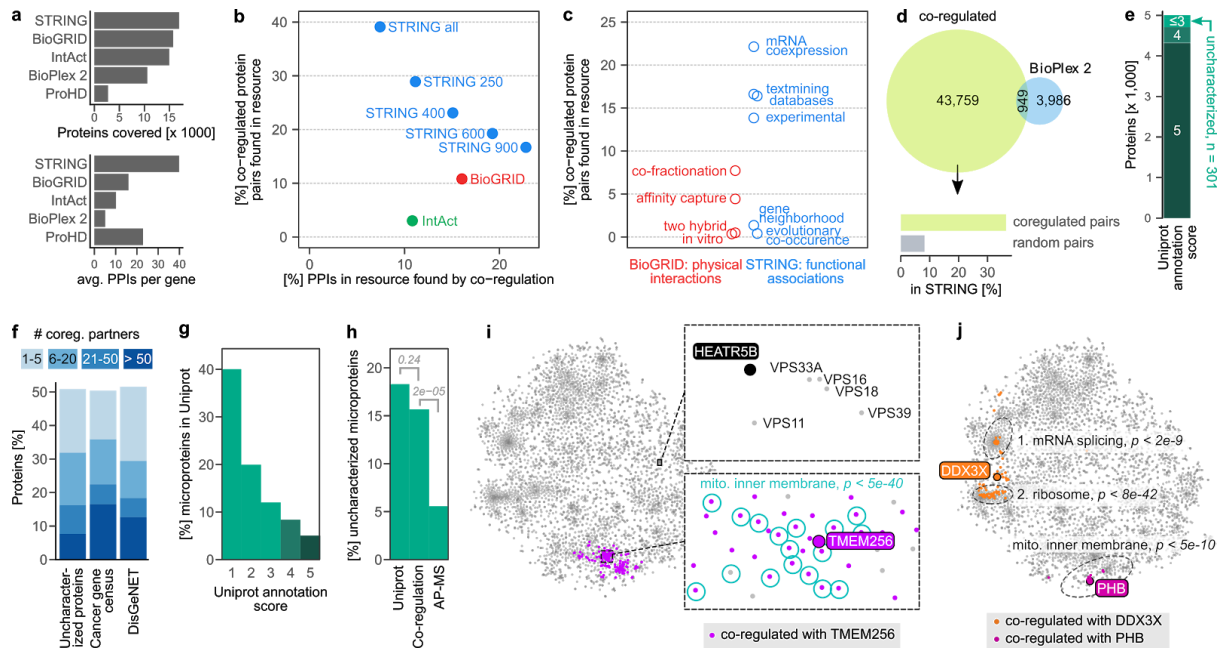
## MAIN FIGURES



484 **Figure 1. The co-regulation map shows functional associations between human**  
485 **proteins.**

486 (a) Assembly of ProteomeHD, which quantifies the protein response to 294 perturbations  
487 using SILAC<sup>45</sup>. Most measurements document protein abundance changes in whole-cell  
488 samples, but in some cases subcellular fractions were enriched to detect low-abundance  
489 proteins. Data were collected from PRIDE<sup>46</sup> and produced in-house. (b) A random set of  
490 experiments from ProteomeHD, showing that groups of proteins with related functions, e.g.  
491 Gene Ontology<sup>52</sup> (GO) biological processes, display similar expression changes. Note that  
492 the fold-changes are often very small. (c) Precision - recall analysis showing that the  
493 treeClust<sup>48,49</sup> algorithm outperforms three correlation-based coexpression measures.  
494 Applying the topological overlap measure (TOM) improves performance further. Annotations  
495 in Reactome<sup>47</sup> were used as gold standard. (d) Co-regulation scores for all protein pairs are  
496 obtained by combining treeClust with TOM. The score distribution is highly skewed. Where

497 an arbitrary threshold is required, the highest-scoring 0.5% of pairs (N = 62,812) are  
498 considered “co-regulated”. (e) Co-regulated protein pairs are strongly enriched for subunits  
499 of the same protein complex, enzymes catalysing consecutive metabolic reactions and  
500 proteins with identical subcellular localization. (f) Most proteins are co-regulated with no or  
501 few other proteins, but many have more than 5 co-regulated partners. (g) Considering  
502 proteins that are co-regulated with  $\geq 10$  proteins, these groups of co-regulated proteins are  
503 almost always enriched in one or more GO terms. (h) The global co-regulation map of  
504 ProteomeHD created using t-Distributed Stochastic Neighbor Embedding (t-SNE)<sup>55,56</sup>.  
505 Distances between proteins indicate how similar their expression patterns are. See  
506 [www.proteomeHD.net](http://www.proteomeHD.net) for an interactive version of the map. (i) The co-regulation map  
507 broadly corresponds to subcellular compartments, and more detailed functional associations  
508 can be observed at higher resolution, as exemplified in subpanels 1-3.



509 **Figure 2. Protein co-regulation complements existing methods and predicts functions**  
 510 **of unknown proteins.**

511 (a) Coverage of protein - protein interactions (PPIs) in comparison to other resources. Top  
 512 barchart shows the number of genes covered, i.e. having at least one PPI above cut-off.  
 513 STRING cut-off used: medium (400). Bottom chart shows the average number of PPIs of  
 514 covered genes. The co-regulation map (ProHD) covers fewer genes than STRING, BioGRID,  
 515 IntAct and BioPlex 2, but covers many associations between those genes. (b) Overlap  
 516 between PPIs discovered by protein co-regulation and PPIs already present in large-scale  
 517 annotation resources that cover both physical (BioGrid<sup>59</sup> and IntAct<sup>58</sup>) and functional  
 518 (STRING<sup>60</sup>) associations. Multiple association score cut-offs were considered for STRING.  
 519 These three resources integrate data from many small and large-scale studies. (c) Coverage  
 520 of co-regulated protein pairs in BioGRID and STRING broken down by the type of functional  
 521 genomics evidence available in each resource. (d) Number of co-regulation links compared  
 522 to PPIs found for the same set of genes by BioPlex 2.0<sup>4</sup>, one of the largest PPI datasets  
 523 reported to date by a single study. Associations unique to co-regulation are strongly enriched  
 524 for links in STRING, compared to random gene pairs. (e) Out of the 5,013 proteins in the  
 525 co-regulation map, 301 have a UniProt annotation score  $\leq 3$  and are thus defined as  
 526 uncharacterized. (f) Connectivity of either uncharacterized proteins or proteins encoded by  
 527 disease genes to well-characterized proteins (annotation score  $\geq 4$ ). 51% of uncharacterized  
 528 proteins have at least one co-regulation partner, 32% have more than five. (g) Barchart  
 529 showing the percentage of all 20,408 human UniProt (SwissProt) proteins that are  
 530 microproteins, i.e. have a molecular weight  $< 15$  kDa. Note that microproteins are heavily  
 531 enriched among less well-characterized proteins. (h) 18% of uncharacterized proteins in  
 532 UniProt are microproteins, compared to 16% of the uncharacterized proteins in the  
 533 co-regulation map and 6% in state-of-the-art AP-MS experiments, represented by BioPlex.  
 534 *P*-values are from one-sided Fisher's Exact test. (i) The uncharacterized microprotein

535 TMEM256 has many co-regulation partners, which are enriched for GO term “mitochondrial  
536 inner membrane” among others. Bonferroni-adjusted  $P$ -value is from a hypergeometric test.  
537 The uncharacterized HEATR5B protein has no co-regulation partners above the default  
538 threshold, but its position in the map nevertheless indicates a potential function. (j) For  
539 multifunctional proteins, co-regulation can reveal a mix of their functions (DDX3X), or their  
540 main function only (prohibitin, PHB). Three representative GO terms are shown.



541  
542  
543  
544  
545  
546  
547  
548  
549  
550  
551  
552  
553  
554  
555  
556  
557  
558  
559  
560  
561  
562  
563  
564  
565  
566  
567  
568  
569  
570  
571  
572  
573  
574  
575  
576

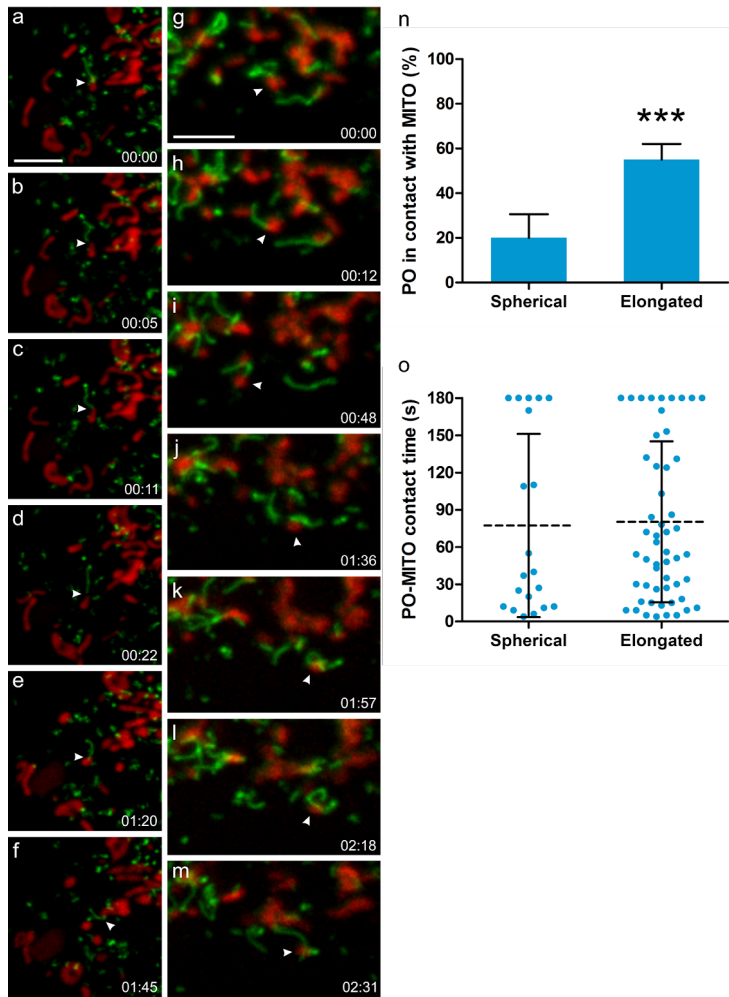


**Figure 3. PEX11 $\beta$  mediates the formation of peroxisomal membrane protrusions which interact with mitochondria in mammalian cells.**

(a-m) COS-7 cells were transfected with PEX11 $\beta$ -EGFP, mitochondria were stained with Mitotracker (red) and cells observed live using a spinning disc microscope. PEX11 $\beta$ , a membrane shaping protein, induces the formation of tubular membrane protrusions from globular peroxisomes. We show here that those membrane protrusions can interact with mitochondria. (a-f) shows a peroxisome which interacts with a mitochondrion via its membrane protrusion (arrowhead), and follows it, occasionally detaching and re-establishing contact before interacting with another mitochondrion (see Supplementary Movie 1). (g-m) shows a mitochondrion (arrowhead) which interacts with a peroxisome via a peroxisomal membrane protrusion. It then detaches and moves away to interact with another peroxisome, which wraps its protrusion around it, before interacting with another mitochondrion (see Supplementary Movie 2). (n) Quantification of interactions between spherical or elongated peroxisomes (PO) with mitochondria (MITO). The average result of 3 independent experiments is shown, error bars indicate standard deviation. (o) Quantification of contact time. Note that elongated PO interact more frequently with MITO than spherical PO, but for similar time periods. PO-MITO interactions are generally long-lasting (see Supplementary Movie 3) (n=200 peroxisomes from 5 different cells). Dotted line indicates the mean, error bars indicate standard deviation. \*\*\*  $P < 0.001$  from a two-tailed unpaired  $t$  test; Time (min:sec). Scale bars, 5  $\mu$ m.

577  
 578  
 579  
 580  
 581  
 582  
 583  
 584  
 585  
 586  
 587  
 588  
 589  
 590  
 591  
 592  
 593  
 594  
 595  
 596  
 597  
 598  
 599  
 600  
 601  
 602  
 603  
 604  
 605  
 606  
 607

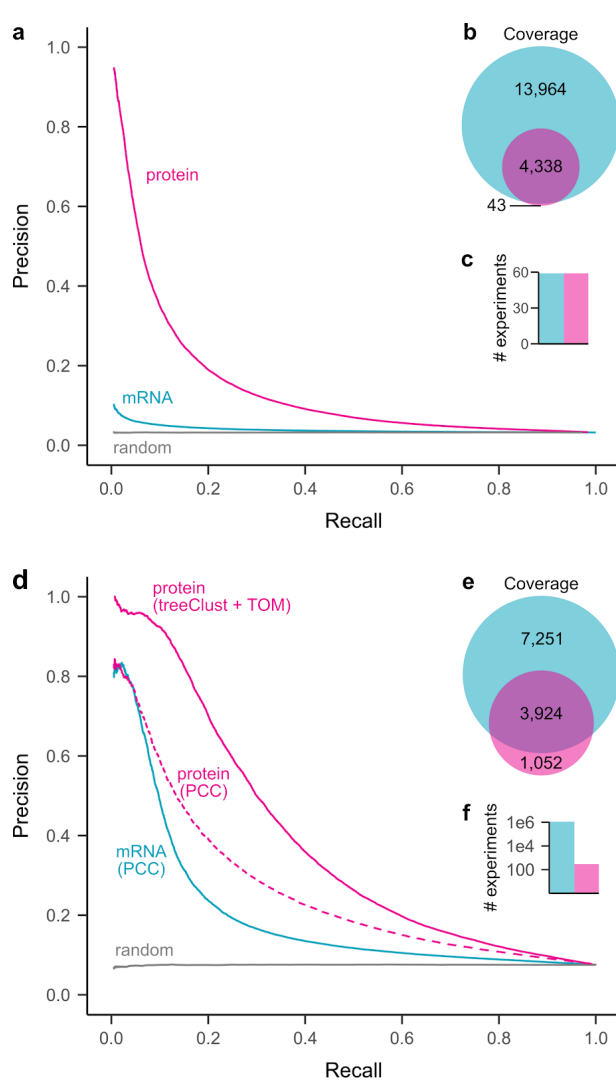


**Figure 4. Protein co-regulation enables higher precision from less data, but has lower coverage than classic mRNA coexpression.**

(a) Precision-recall analysis of treeClust machine-learning on a subset of ProteomeHD, that is 59 samples for which matching RNA-seq data were available from a separate study<sup>85</sup>. Reactome pathways were used as gold standard for true functional associations (proteins found in same pathway) and false associations (never found in same pathway). Only annotated genes covered by both datasets were considered for PR analysis (n = 2,901). (b) Venn diagram showing number of genes covered by each analysis. (c) Barchart showing number of experiments the curves are based on. (d) Similar precision-recall analysis of treeClust machine-learning on the full ProteomeHD database, in comparison to Pearson correlation obtained by STRING<sup>60</sup> on the basis of one million human mRNA profiling samples deposited in the NCBI Gene Expression Omnibus<sup>86</sup> ("mRNA / PCC"). Protein co-regulation outperforms mRNA

correlation despite being based on orders-of-magnitude less data. This is partially due to the use of machine-learning, as predicting associations from ProteomeHD using PCC decreases performance markedly ("protein / PCC"). Only annotated genes covered by both datasets were considered for the PR analysis (n = 2,743). (e, f) same as (b, c).

## 608 ONLINE METHODS

### 609 General data analysis and code availability

610 Data analysis was performed in R<sup>90</sup>. R scripts and input files required to reproduce the  
611 results of this manuscript are available in the following GitHub repository:  
612 <https://github.com/Rappsilber-Laboratory/ProteomeHD>. The R package `data.table`<sup>91</sup> was  
613 used for fast data processing. Figures were prepared using `ggplot2`<sup>92</sup>, `gridExtra`<sup>93</sup>, `cowplot`<sup>94</sup>  
614 and `viridis`<sup>95</sup>.

### 615 Data selection for ProteomeHD

616 MS raw data were produced in-house or downloaded from the PRIDE repository<sup>46</sup>. Only  
617 experiments fulfilling the following inclusion criteria were considered:

618 (1) Comparative proteomics experiments, i.e. relative protein quantitations of two or  
619 more biological states. For example, cells treated with an inhibitor vs. mock control. (2)  
620 Biological - not biochemical - comparisons, i.e. fold-changes must have been brought about  
621 *in vivo*, not by differential biochemical purification. For example, SILAC-labelled cells were  
622 treated with inhibitor or mock control, harvested and combined, and chromatin was enriched  
623 on the combined sample. In such cases any observed fold-change reflects the response to  
624 the inhibitor in the living cell, for example a protein re-localising from cytoplasm onto  
625 chromatin. We did not consider experiments that compared, for example, a whole-cell lysate  
626 with a chromatin-enriched fraction, as this would measure the impact of the biochemical  
627 enrichment rather than a biological event. (3) Quantitation by “stable isotope labeling by  
628 amino acids in cell culture” (SILAC)<sup>45</sup>. (4) Samples of human origin.

629 In addition to these conceptual considerations, the following restrictions were  
630 imposed by the data processing pipeline: (5) The SILAC mass shift introduced by heavy  
631 arginine must be distinct from heavy lysine. (6) Raw data acquired on an Orbitrap mass  
632 spectrometer. (7) Samples alkylated with iodoacetamide, resulting in carbamidomethylation  
633 of cysteines.

634 In total, we considered 294 experiments (SILAC ratios) from 31 projects. A full list of  
635 these is provided in Supplementary Table 2, which also includes the PRIDE identifiers of all  
636 previously published datasets.

### 637 In-house data collection

638 80 experiments were performed in-house and analyzed chromatin-enriched samples. Of  
639 these, 65 measured the effect of growth factors, radiation and other perturbations on  
640 interphase chromatin, which was prepared using Chromatin Enrichment for Proteomics  
641 (ChEP)<sup>96</sup>. About half of these experiments had previously been published<sup>36</sup>. Another 15  
642 experiments documented perturbations specifically on freshly replicated chromatin, which  
643 was prepared using Nascent Chromatin Capture (NCC)<sup>97</sup>. All mass spectrometry raw files  
644 generated in-house have been deposited to the ProteomeXchange Consortium  
645 (<http://proteomecentral.proteomexchange.org>) via the PRIDE partner repository<sup>46</sup> with the  
646 dataset identifier PXD008888 (reviewer login: username “reviewer64164@ebi.ac.uk”,  
647 password “hQPX4xZd”).

## 648 **MS raw data processing**

649 The 5,288 MS raw files were processed using MaxQuant 1.5.2.8<sup>98</sup> on a Dell PowerEdge  
650 R920 server. The following default MaxQuant search parameters were used: MS1 tolerance  
651 for the first Andromeda search: 20 ppm, MS1 tolerance for the main Andromeda search: 4.5  
652 ppm, FTMS MS2 match tolerance: 20 ppm, ITMS MS2 match tolerance: 0.5 Da, Variable  
653 modifications: acetylation of protein N-termini, oxidation of methionine, Fixed modifications:  
654 carbamidomethylation of cysteine, Decoy mode set to reverse, Minimum peptide length: 7  
655 and Max missed cleavages set to 2. The following non-default settings were used: In  
656 group-specific parameters, match type was set to “No matching”. In global parameters,  
657 “Re-quantify” was enabled, minimum ratio count was set to 1 and “Discard unmodified  
658 counterpart peptide” was disabled. Also in global parameters, writing of large tables was  
659 disabled. SILAC labels were set as group-specific parameters as indicated in Supplementary  
660 Table 2. Canonical and isoform protein sequences were downloaded from UniProt<sup>61</sup> on 28th  
661 May 2015, considering only reviewed SwissProt entries that were part of the human  
662 proteome. Unprocessed MaxQuant result tables, including peptide evidence data, have been  
663 deposited into the PRIDE repository PXD008888.

664 Protein fold-changes were extracted from the MaxQuant proteinGroups file returned  
665 by MaxQuant. Non-normalized SILAC ratios were considered for downstream analysis, log2  
666 transformed and median-normalised. From triple labelling experiments, the heavy/light and  
667 medium/light ratios - but not the heavy/medium ratios - were considered. Proteins detected  
668 in less than 4 experiments were discarded, as were proteins labeled as contaminants,  
669 reverse hits and those only identified by a modification site. The resulting data matrix,  
670 ProteomeHD, can be downloaded as Supplementary Table 1.

## 671 **Calculation of treeClust dissimilarities**

672 It is common in gene coexpression studies to remove genes that were detected in less than  
673 half of the samples from the analysis. However, given the unusually large size of  
674 ProteomeHD we chose a different arbitrary cut-off, excluding proteins that were detected in  
675 less than 95 (about a third) of the 294 experiments. For the remaining 5,013 proteins in  
676 ProteomeHD we used the treeClust<sup>48</sup> R package to calculate all 12,562,578 pairwise  
677 dissimilarities. Note that treeClust was designed not only to measure inter-point  
678 dissimilarities but also to perform clustering<sup>48,49</sup>. However, in this study we use it only to  
679 calculate dissimilarities, via the treeClust.dist function. The dissimilarity specifier was set to  
680 d.num = 2, so that dissimilarities are weighted according to tree quality. We optimised two  
681 hyperparameters of treeClust and rpart, which is the routine treeClust uses to create  
682 decision trees. These were treeClust’s serule argument, which defines to extent to which  
683 trees are pruned, and rpart’s complexity (cp) parameter, which describes the improved fit  
684 required to attempt a split. A grid search was performed against the Reactome gold standard  
685 (see below) and the area under precision - recall curves was used to identify optimal  
686 parameter settings. They were determined to be serule = 1.8 and cp = 0.105, providing  
687 approximately a 10% performance improvement over treeClust’s default settings.

## 688 **Protein co-regulation scores**

689 To calculate the final pairwise co-regulation scores, treeClust dissimilarities were  
690 transformed further. First, they were turned into similarities, i.e.  $1 - \text{treeClust dissimilarity}$ .  
691 Using the WGCNA<sup>99,100</sup> R package, we then performed a sigmoid transformation of these  
692 treeClust similarities, creating an adjacency matrix. The settings of parameters  $\mu$  and  $\alpha$   
693 for this transformation were optimised in a grid search against the Reactome gold standard,  
694 using the area under precision - recall curves as readout. In a third step, the adjacency  
695 matrix was transformed into a topological overlap matrix using WGCNA's TOMsimilarity  
696 function, with the TOMDenom parameter set to "mean". These TOM similarities are the  
697 co-regulation scores used throughout our analysis. Co-regulation scores for all of our  
698 12,562,578 protein pairs can be downloaded from the PRIDE repository PXD008888.

699 While the co-regulation score is continuous, some analyses benefitted from a  
700 simplified categorical approach. For these cases we arbitrarily defined the highest-scoring  
701 0.5% of protein pairs as "co-regulated pairs" and the remaining 99.5% of pairs as "not  
702 co-regulated pairs". A list of all 62,812 co-regulated protein pairs is available as  
703 Supplementary Table 3.

## 704 **Reactome gold standard**

705 A gold standard set of reference proteins was defined using Reactome<sup>47</sup>. Bona fide  
706 functionally associated protein pairs (true positives) were defined as protein pairs found in  
707 the same "detailed" Reactome pathway. This was inferred from the file UniProt2Reactome.txt  
708 (available at <https://reactome.org/download-data>), where each protein is annotated to the  
709 lowest level subset of Reactome pathways. To make sure that only closely related protein  
710 pairs were assigned the "true positive" label, we excluded two pathways that were composed  
711 of > 200 proteins. We defined protein pairs that are not functionally associated (false  
712 positives) as proteins that are never in the same Reactome pathway, at any annotation level.  
713 This was inferred from UniProt2Reactome\_All\_Levels.txt (also available at  
714 <https://reactome.org/download-data>), a file that maps proteins to all levels of the Reactome  
715 pathway hierarchy. A copy of this gold standard is available in the Github repository noted  
716 above.

## 717 **Comparison of treeClust and correlation metrics**

718 Pearson's correlation coefficients (PCC) and Spearman's rank correlation coefficients ( $\rho$ )  
719 were obtained using the cor function in R, for the same protein pairs covered by the  
720 treeClust analysis. Biweight mid-correlation coefficients (bicor) were calculated with default  
721 settings using the R package WGCNA<sup>100,101</sup>. Changing the maxPOutliers parameter of the  
722 bicor function did not improve performance. Precision - recall (PR) analysis was performed  
723 with the ROCR package<sup>102</sup> using true and false positive pairs compiled from annotation in  
724 Reactome (see paragraph Reactome gold standard). The random classifier was created by  
725 scrambling co-regulation scores.

## 726 **t-SNE visualization**

727 To visualize ProteomeHD as a 2D co-regulation map, co-regulation scores were subjected to  
728 t-Distributed Stochastic Neighbor Embedding (t-SNE)<sup>55,56</sup> using the Rtsne<sup>103</sup> package for R.

729 The theta parameter was set to zero to calculate the exact embedding. The perplexity  
730 parameter was set to 50, up from the default of 30, to account for the large size of the  
731 co-regulation dataset. 1,500 iterations were performed. However, visual comparison of the  
732 t-SNE maps showed that these parameter adaptations provided only a marginal  
733 improvement over the default settings. Organelles were labelled based on subcellular  
734 locations assigned by UniProt<sup>61</sup> to these proteins, zoom regions were annotated manually  
735 based on available literature. Plot coordinates and annotations are available as  
736 Supplementary Table 4.

### 737 **Network visualizations**

738 In addition to t-SNE, the protein co-regulation matrix was also visualized as an undirected,  
739 weighted network using the igraph<sup>104</sup> and GGally<sup>105</sup> packages in R. The network contains the  
740 same 5,013 proteins as the co-regulation map, but only considers links above the arbitrary  
741 co-regulation threshold, i.e. between the top-scoring 0.5% of protein pairs. For these pairs,  
742 the network edges are weighted by the co-regulation score. A set of common network layout  
743 algorithms were deployed through the sna (social network analysis)<sup>106</sup> R package.

### 744 **Testing for co-functionality among of co-regulated proteins**

745 To test if protein co-regulation reflects co-function we defined three sets of “functionally  
746 related” protein pairs (subunits of the same protein complexes, enzymes catalyzing  
747 consecutive metabolic reactions and proteins with identical subcellular localization) as  
748 previously described<sup>25</sup>.

749 To test larger groups (not pairs) of co-regulated proteins for functional enrichment, we  
750 analyzed enrichment of Gene Ontology terms using the topGO<sup>107</sup> R package. For each  
751 protein we tested the group of its co-regulation partners for GO term enrichment. Because  
752 some proteins are co-regulated with no or very few other proteins, we restricted the analysis  
753 to proteins that are co-regulated with at least 10 proteins. The three aspects (Biological  
754 process, Molecular function, Cellular component) of GO were downloaded from QuickGO<sup>108</sup>  
755 with taxon set to human and qualifier to null. Rather than the whole proteome, only proteins  
756 that were included in the treeClust analysis and had GO annotations were used as the gene  
757 “universe” or background for the topGO analysis. Enrichment of GO terms among protein  
758 co-regulation groups was tested considering GO graph structure and using a Fisher’s exact  
759 test.

### 760 **Annotation of the co-regulation map**

761 Proteins localizing to specific subcellular compartments were downloaded from UniProt<sup>61</sup>  
762 using the following tags: Nucleus (SL-0191), Nucleolus (SL-0188), Endoplasmic reticulum  
763 (SL-0095), Mitochondrion (SL-0173), Cytoplasm (SL-0086), Secreted (SL-0243). Proteins  
764 and protein complexes in zoom regions (Fig. 1i) were annotated individually based on the  
765 available literature.

### 766 **Creating the www.proteomeHD.net framework**

767 The ProteomeHD online application was written in Python Flask web framework. The  
768 interactive plots are generated using Bokeh visualization library for Python

769 (<https://github.com/bokeh/bokeh>). The Gene Ontology and KEGG enrichment statistics are  
770 obtained from a STRING<sup>60</sup> server using an API call with maximally top 100 proteins  
771 co-regulated with the query. Only significantly enriched terms (hypergeometric test,  
772 Bonferroni adjusted  $P$  value  $< 0.1$ ) are displayed.

### 773 **Comparison to orthogonal methods**

774 Physical protein-protein-interactions (PPIs) detected by a comprehensive range of small-  
775 and large-scale methods were assessed using BioGRID<sup>59</sup>, version 3.4.152. Data from  
776 IntAct<sup>58</sup> were used as a smaller but curated resource of physical PPIs. Functional protein  
777 associations mapped by a large range of methods and publications were inferred from  
778 STRING<sup>60</sup>, version 10.5. Note that the protein co-regulation scores described here are only  
779 used by STRING starting with version 11<sup>75</sup>. BioPlex 2.0<sup>4</sup> served as an example for physical  
780 interactions mapped by a single project.

### 781 **Annotation of uncharacterized and disease genes**

782 Proteins were defined as “uncharacterized” on the basis of having an annotation score  $\leq 3$  in  
783 UniProt<sup>61</sup>. The UniProt annotation score is a heuristic measure of the annotation state of a  
784 protein, expressed as a 5-point system ([www.uniprot.org/help/annotation\\_score](http://www.uniprot.org/help/annotation_score)). The score  
785 combines various types and layers of UniProt annotation, and weights manually curated  
786 evidence higher than automated annotation. It may not always agree with the state of  
787 “characterization” that field experts would assign to the same protein. However, as an  
788 unbiased, data-driven approach we believe the UniProt annotation score is better suited to  
789 systematically identify uncharacterized proteins than manual annotation could be. Even with  
790 a systematic way of measuring the degree of annotation, the definition of what constitutes an  
791 “uncharacterised” protein is an arbitrary one. We chose “3 points or less” as the  
792 “uncharacterized” cut-off, because the available information for such proteins tends to be  
793 very vague, e.g. a sequence-based prediction as “multi-pass membrane protein”. In contrast,  
794 we found that the biological function of most 4-star proteins could be established reasonably  
795 well from the available literature.

796 The Cancer Gene Census, i.e. genes that can cause cancer when mutated, was  
797 curated by COSMIC (Catalogue Of Somatic Mutations In Cancer, version 81)<sup>62</sup>. DisGeNET  
798 was used as a comprehensive, curated list of human gene - disease associations<sup>63</sup>.

### 799 **Comparison of mRNA and protein expression profiling**

800 For the comparison of matched samples and proteins we considered mRNA and protein  
801 expression changes across 59 lymphoblastoid cell lines (Fig. 4a). The protein fold-changes  
802 are part of ProteomeHD and were originally published by Battle and colleagues<sup>30</sup>.  
803 RNA-sequencing data for the same cell lines and proteins were also previously reported<sup>85</sup>.  
804 We used the RNA-sequencing data to calculate mRNA fold-changes relative to a 60th cell  
805 line, which was the same cell line used as a SILAC reference for the protein expression data.  
806 The combined mRNA and protein dataset has been described in more detail elsewhere<sup>25</sup>.  
807 Fold-changes for genes covered by both the transcriptomics and proteomics analysis were  
808 subjected to treeClust learning (default parameters) and PR curves were obtained as  
809 described above.

810 For a more comprehensive comparison we considered protein associations predicted  
811 using treeClust learning or PCC on the basis of all 294 SILAC ratios in ProteomeHD (Fig.  
812 4b). This was compared to mRNA associations inferred by PCC on the basis of all human  
813 mRNA expression data processed by STRING. STRING's state-of-the-art mRNA  
814 coexpression analysis pipeline considers all microarray and RNA-sequencing data deposited  
815 in the GEO repository<sup>86</sup>, resulting in one of the largest mRNA coexpression analyses  
816 available to date<sup>60,87</sup>. Note that for this comparison we did not use the STRING coexpression  
817 score, which is calibrated against the KEGG database, but the original uncalibrated  
818 Pearson's correlations, which were kindly provided by Damian Szklarczyk. STRING PCCs  
819 are calculated separately for one- and two-channel microarrays and RNA-sequencing  
820 experiments. We used the average of these for the precision - recall analysis, which  
821 performed better than any individual experiment type.

### 822 **Validation of treeClust and t-SNE on the cancer proteomics dataset**

823 Lapek *et al* measured the abundances for 6,911 proteins in 41 different breast cancer cell  
824 lines<sup>20</sup>. These data are available as Supplementary Table 2 (tab 3) of their report. As  
825 described by Lapek *et al*, we converted the protein intensities into log2 fold-changes over the  
826 median intensity measured for each protein across all cell lines. We then calculated  
827 Pearson's, Spearman's rank and bicor correlations for all possible protein pairs, as for  
828 ProteomeHD. The Spearman's correlation coefficients obtained in this way are identical to  
829 the ones obtained by Lapek *et al* using the cor.prob function (Supplementary Table 6 in their  
830 report<sup>20</sup>). We also determined treeClust co-regulation scores for all protein pairs. However,  
831 treeClust can only grow one decision tree per input variable, i.e. 41 in this dataset, which  
832 would be too few for it to perform properly. To circumvent this, we forced treeClust to  
833 generate 1,000 decision trees by applying it iteratively. We created 100 treeClust forests,  
834 each generated with a random subset of 10 of the 41 variables, and used the average  
835 co-regulation score for downstream analysis. Precision-recall analysis using a Reactome  
836 gold standard and t-SNE visualization were performed as described above. The CORUM  
837 protein complexes displayed in Lapek *et al*'s Figure 2, reported in their Supplementary Table  
838 7<sup>20</sup>, were color-coded in the co-regulation map.

### 839 **Comparison of protein co-regulation and co-occurrence**

840 Two different approaches were used to measure protein co-occurrence in ProteomeHD.  
841 First, the Jaccard / Tanimoto similarity coefficient<sup>53</sup> was calculated using the Jaccard  
842 package for R. Second, a binary version of ProteomeHD was created, where all SILAC ratios  
843 were represented by 1s ("protein quantified") and all missing values were turned to 0s  
844 ("protein not quantified"). Subsequently, treeClust dissimilarities were re-calculated based on  
845 this binary version of ProteomeHD. The performance of these different metrics was  
846 assessed by a precision - recall analysis as described above.

### 847 **Plasmids, siRNA, and antibodies**

848 For cloning of peroxisome-targeted Miro1, the C-terminal TMD and tail of Myc-Miro1 (kindly  
849 provided by P. Aspenström, Karolinska Institute, Sweden) was exchanged by a PEX26/ALDP  
850 fragment previously shown to target proteins to the peroxisome membrane<sup>81</sup>. PEX11β-EGFP



851 was kindly provided by G. Dodt (Univ. of Tuebingen, Germany). PEX11 $\beta$  siRNA (AUU AGG  
852 GUG AGA AUA GAC AGG AUGG) (Eurofins) was previously verified<sup>109</sup>. Control siRNA  
853 (si-GENOME nontargeting siRNA pool #2) was obtained from GE Healthcare  
854 (D-001206-14-05). Antibodies used were as follows: rabbit polyclonal antibody against  
855 PEX14 (1:1400, kindly provided by D. Crane, Griffith University, Australia); mouse  
856 monoclonal antibody 9E10 against the Myc epitope (1:200, Santa Cruz Biotechnology, Inc.,  
857 sc-40), rabbit monoclonal antibody against PEX11 $\beta$  (1:1000, Abcam, ab181066); rabbit  
858 polyclonal antibody against GAPDH (1:2000, ProSci3783). Secondary anti-IgG antibodies  
859 against rabbit (Alexa 594, 1:1000, Molec. Probes/Life Technol. A21207) and mouse (Alexa  
860 488, 1:400, Molec. Probes/Life Technol. A21202) were obtained from ThermoFisher  
861 Scientific. HRP-coupled donkey polyclonal antibody against rabbit IgG (1:5000) was  
862 obtained from Biorad (172-1013).

### 863 **Cell culture and transfection**

864 COS-7 cells (African green monkey kidney cells; ATCC CRL-1651), and PEX5 deficient  
865 fibroblasts (kindly provided by H. Waterham, AMC, University of Amsterdam, NL) were  
866 cultured in DMEM (high glucose, 4.5 g/L) supplemented with 10% FBS, 100 U/ml penicillin  
867 and 100  $\mu$ g/ml streptomycin at 37°C (5% CO<sub>2</sub>, 95% humidity) (HERACell 240i CO<sub>2</sub>  
868 incubator). COS-7 cells were transfected using diethylaminoethyl-dextran (Sigma-Aldrich).  
869 dPEX5 fibroblasts have enlarged peroxisomes, which facilitates the visualization of  
870 membrane extensions. For transfection of dPEX5 fibroblasts, the Neon® Transfection  
871 System (Thermo Fisher Scientific) was used following the manufacturer's protocol. Briefly,  
872 cells (seeded 24h before transfection) were washed once with PBS and trypsinized using  
873 TrypLE Express. Trypsinized cells were resuspended in complete medium, pelleted by  
874 centrifugation, and washed with PBS. The cells were once again centrifuged and carefully  
875 resuspended in 110  $\mu$ l buffer R. For each condition, 4  $\times$  10<sup>5</sup> cells were mixed with the DNA  
876 construct (5  $\mu$ g) or with 100 nM siRNA. Cells were microporated using a 100  $\mu$ l Neon tip with  
877 the following settings: 1400 V, 20 ms, one pulse. Microporated cells were immediately  
878 seeded into plates with prewarmed complete medium (without antibiotics) and incubated at  
879 37°C with 5% CO<sub>2</sub> and 95% humidity. The efficiency of silencing was monitored by  
880 immunoblotting of cell lysates and confirmed as previously reported<sup>109</sup>.

### 881 **Immunofluorescence and microscopy**

882 Cells grown on glass coverslips were processed for immunofluorescence 24h after  
883 transfection. Cells were fixed for 20 min with 4% paraformaldehyde in PBS (pH 7.4),  
884 permeabilized with 0.2% Triton X-100, and blocked with 1% BSA, each for 10 min.  
885 Incubation with primary and secondary antibodies took place for 1h each in a humid  
886 chamber. Coverslips were washed with ddH<sub>2</sub>O to remove PBS and mounted with Mowiol  
887 medium on glass slides. All immunofluorescence steps were performed at room temperature  
888 and cells were washed three times with PBS between each individual step. Cell imaging was  
889 performed using an IX81 microscope (Olympus) equipped with an UPlanSApo 100 $\times$ /1.40 oil  
890 objective (Olympus). Digital images were taken with a CoolSNAP HQ2 CCD camera and  
891 adjusted for contrast and brightness using the Olympus Soft Imaging Viewer software and  
892 MetaMorph 7 (Molecular Devices). For live-cell imaging, COS-7 cells were plated in 3.5 cm

893 diameter glass bottom dishes (Cellvis). MitoTracker Red CMXRos (Life Technologies) at 100  
894 nM was used for visualisation of mitochondria. Live-cell imaging data was collected using an  
895 Olympus IX81 microscope equipped with a Yokogawa CSUX1 spinning disk head,  
896 CoolSNAP HQ2 CCD camera, 60 x/1.35 oil objective. Digital images were taken and  
897 processed using VisiView software (Visitron Systems, Germany). Prior to image acquisition,  
898 a controlled temperature chamber was set-up on the microscope stage at 37°C, as well as  
899 an objective warmer. During image acquisition, cells were kept at 37°C and in  
900 CO<sub>2</sub>-independent medium (HEPES buffered). 200 stacks of 9 planes (0.5 µm thickness, 100  
901 ms exposure) were taken in a continuous stream. All conditions and laser intensities were  
902 kept between experiments.

### 903 **Quantification and statistical analysis of peroxisome morphology and interaction**

904 Analysis of statistical significance was performed using GraphPad Prism 5 software. A  
905 two-tailed unpaired *t* test was used to determine statistical difference against the indicated  
906 group. \**P* < 0.05, \*\**P* < 0.01, \*\*\**P* < 0.001. For analysis of peroxisome morphology, a  
907 minimum of 150 cells were examined per condition, and organelle parameters (e.g.  
908 membrane protrusions) were microscopically assessed in at least three independent  
909 experiments. The analysis was made blind and in different areas of the coverslip. Organelle  
910 interaction and contact time were analysed manually from live-cell imaging data using  
911 MetaMorph 7 (Molecular Devices). A region of interest (ROI) was drawn in different areas of  
912 the cell. Spherical and elongated peroxisomes within the ROI were tracked over the whole  
913 time course, and the frequency and duration of contacts monitored. Multiple interactions of  
914 the same peroxisome with mitochondria were treated as separate events. Data are  
915 presented as mean ± SD.

916 **REFERENCES**

- 917 1. Gavin, A.-C. *et al.* Proteome survey reveals modularity of the yeast cell machinery.  
918 *Nature* **440**, 631–636 (2006).
- 919 2. Havugimana, P. C. *et al.* A census of human soluble protein complexes. *Cell* **150**,  
920 1068–1081 (2012).
- 921 3. Hein, M. Y. *et al.* A human interactome in three quantitative dimensions organized by  
922 stoichiometries and abundances. *Cell* **163**, 712–723 (2015).
- 923 4. Huttlin, E. L. *et al.* Architecture of the human interactome defines protein communities  
924 and disease networks. *Nature* **545**, 505–509 (2017).
- 925 5. Rolland, T. *et al.* A proteome-scale map of the human interactome network. *Cell* **159**,  
926 1212–1226 (2014).
- 927 6. Dunkley, T. P. J., Watson, R., Griffin, J. L., Dupree, P. & Lilley, K. S. Localization of  
928 organelle proteins by isotope tagging (LOPIT). *Mol. Cell. Proteomics* **3**, 1128–1134  
929 (2004).
- 930 7. Foster, L. J. *et al.* A mammalian organelle map by protein correlation profiling. *Cell* **125**,  
931 187–199 (2006).
- 932 8. Christoforou, A. *et al.* A draft map of the mouse pluripotent stem cell spatial proteome.  
933 *Nat. Commun.* **7**, 8992 (2016).
- 934 9. Thul, P. J. *et al.* A subcellular map of the human proteome. *Science* **356**, (2017).
- 935 10. Costanzo, M. *et al.* A global genetic interaction network maps a wiring diagram of  
936 cellular function. *Science* **353**, (2016).
- 937 11. Mülleder, M. *et al.* Functional Metabolomics Describes the Yeast Biosynthetic  
938 Regulome. *Cell* **167**, 553–565.e12 (2016).
- 939 12. Schena, M., Shalon, D., Davis, R. W. & Brown, P. O. Quantitative monitoring of gene  
940 expression patterns with a complementary DNA microarray. *Science* **270**, 467–470  
941 (1995).
- 942 13. DeRisi, J. L., Iyer, V. R. & Brown, P. O. Exploring the metabolic and genetic control of  
943 gene expression on a genomic scale. *Science* **278**, 680–686 (1997).
- 944 14. Eisen, M. B., Spellman, P. T., Brown, P. O. & Botstein, D. Cluster analysis and display of  
945 genome-wide expression patterns. *Proc. Natl. Acad. Sci. U. S. A.* **95**, 14863–14868  
946 (1998).
- 947 15. Kim, S. K. *et al.* A gene expression map for *Caenorhabditis elegans*. *Science* **293**,  
948 2087–2092 (2001).
- 949 16. Hughes, T. R. *et al.* Functional discovery via a compendium of expression profiles. *Cell*  
950 **102**, 109–126 (2000).
- 951 17. Stuart, J. M., Segal, E., Koller, D. & Kim, S. K. A gene-coexpression network for global  
952 discovery of conserved genetic modules. *Science* **302**, 249–255 (2003).
- 953 18. Singh, S. A. *et al.* Co-regulation proteomics reveals substrates and mechanisms of  
954 APC/C-dependent degradation. *EMBO J.* **33**, 385–399 (2014).
- 955 19. Wang, J. *et al.* Proteome Profiling Outperforms Transcriptome Profiling for Coexpression  
956 Based Gene Function Prediction. *Mol. Cell. Proteomics* **16**, 121–134 (2017).
- 957 20. Lapek, J. D., Jr *et al.* Detection of dysregulated protein-association networks by  
958 high-throughput proteomics predicts cancer vulnerabilities. *Nat. Biotechnol.* **35**, 983–989  
959 (2017).

- 960 21. Liu, Y., Beyer, A. & Aebersold, R. On the Dependency of Cellular Protein Levels on  
961 mRNA Abundance. *Cell* **165**, 535–550 (2016).
- 962 22. Wilhelm, M. *et al.* Mass-spectrometry-based draft of the human proteome. *Nature* **509**,  
963 582–587 (2014).
- 964 23. Fortelny, N., Overall, C. M., Pavlidis, P. & Freue, G. V. C. Can we predict protein from  
965 mRNA levels? *Nature* **547**, E19–E20 (2017).
- 966 24. Batada, N. N., Urrutia, A. O. & Hurst, L. D. Chromatin remodelling is a major source of  
967 coexpression of linked genes in yeast. *Trends Genet.* **23**, 480–484 (2007).
- 968 25. Kustatscher, G., Grabowski, P. & Rappsilber, J. Pervasive coexpression of spatially  
969 proximal genes is buffered at the protein level. *Mol. Syst. Biol.* **13**, 937 (2017).
- 970 26. Hurst, L. D. It's easier to get along with the quiet neighbours. *Mol. Syst. Biol.* **13**, 943  
971 (2017).
- 972 27. Raj, A., Peskin, C. S., Tranchina, D., Vargas, D. Y. & Tyagi, S. Stochastic mRNA  
973 synthesis in mammalian cells. *PLoS Biol.* **4**, e309 (2006).
- 974 28. Ebisuya, M., Yamamoto, T., Nakajima, M. & Nishida, E. Ripples from neighbouring  
975 transcription. *Nat. Cell Biol.* **10**, 1106–1113 (2008).
- 976 29. Khan, Z. *et al.* Primate transcript and protein expression levels evolve under  
977 compensatory selection pressures. *Science* **342**, 1100–1104 (2013).
- 978 30. Battle, A. *et al.* Genomic variation. Impact of regulatory variation from RNA to protein.  
979 *Science* **347**, 664–667 (2015).
- 980 31. Geiger, T., Cox, J. & Mann, M. Proteomic changes resulting from gene copy number  
981 variations in cancer cells. *PLoS Genet.* **6**, e1001090 (2010).
- 982 32. Stingele, S. *et al.* Global analysis of genome, transcriptome and proteome reveals the  
983 response to aneuploidy in human cells. *Mol. Syst. Biol.* **8**, 608 (2012).
- 984 33. Dephoure, N. *et al.* Quantitative proteomic analysis reveals posttranslational responses  
985 to aneuploidy in yeast. *Elife* **3**, e03023 (2014).
- 986 34. Ohta, S. *et al.* The protein composition of mitotic chromosomes determined using  
987 multiclassifier combinatorial proteomics. *Cell* **142**, 810–821 (2010).
- 988 35. Wu, L. *et al.* Variation and genetic control of protein abundance in humans. *Nature* **499**,  
989 79–82 (2013).
- 990 36. Kustatscher, G. *et al.* Proteomics of a fuzzy organelle: interphase chromatin. *EMBO J.*  
991 **33**, 648–664 (2014).
- 992 37. Wu, Y. *et al.* Multilayered genetic and omics dissection of mitochondrial activity in a  
993 mouse reference population. *Cell* **158**, 1415–1430 (2014).
- 994 38. Kustatscher, G., Grabowski, P. & Rappsilber, J. Multiclassifier combinatorial proteomics  
995 of organelle shadows at the example of mitochondria in chromatin data. *Proteomics* **16**,  
996 393–401 (2016).
- 997 39. Okada, H., Ebhardt, H. A., Vonesch, S. C., Aebersold, R. & Hafen, E. Proteome-wide  
998 association studies identify biochemical modules associated with a wing-size phenotype  
999 in *Drosophila melanogaster*. *Nat. Commun.* **7**, 12649 (2016).
- 1000 40. Williams, E. G. *et al.* Systems proteomics of liver mitochondria function. *Science* **352**,  
1001 aad0189 (2016).
- 1002 41. Gupta, S., Turan, D., Tavernier, J. & Martens, L. The online Tabloid Proteome: an  
1003 annotated database of protein associations. *Nucleic Acids Res.* (2017).

- 1004 doi:10.1093/nar/gkx930
- 1005 42. Rieckmann, J. C. *et al.* Social network architecture of human immune cells unveiled by  
1006 quantitative proteomics. *Nat. Immunol.* **18**, 583–593 (2017).
- 1007 43. Kim, M.-S. *et al.* A draft map of the human proteome. *Nature* **509**, 575–581 (2014).
- 1008 44. Uhlén, M. *et al.* Proteomics. Tissue-based map of the human proteome. *Science* **347**,  
1009 1260419 (2015).
- 1010 45. Ong, S.-E. *et al.* Stable isotope labeling by amino acids in cell culture, SILAC, as a  
1011 simple and accurate approach to expression proteomics. *Mol. Cell. Proteomics* **1**,  
1012 376–386 (2002).
- 1013 46. Vizcaíno, J. A. *et al.* 2016 update of the PRIDE database and its related tools. *Nucleic*  
1014 *Acids Res.* **44**, D447–56 (2016).
- 1015 47. Fabregat, A. *et al.* The Reactome pathway Knowledgebase. *Nucleic Acids Res.* **44**,  
1016 D481–7 (2016).
- 1017 48. Buttrely, S. E. & Whitaker, L. R. treeClust: an R package for tree-based clustering  
1018 dissimilarities. *The R Journal* **7**, 227–236 (2015).
- 1019 49. Buttrely, S. E. & Whitaker, L. R. A scale-independent, noise-resistant dissimilarity for  
1020 tree-based clustering of mixed data. *NPS Technical Report Archive* (2016). Available at:  
1021 <https://calhoun.nps.edu/handle/10945/48615>.
- 1022 50. Ravasz, E., Somera, A. L., Mongru, D. A., Oltvai, Z. N. & Barabási, A. L. Hierarchical  
1023 organization of modularity in metabolic networks. *Science* **297**, 1551–1555 (2002).
- 1024 51. Yip, A. M. & Horvath, S. Gene network interconnectedness and the generalized  
1025 topological overlap measure. *BMC Bioinformatics* **8**, 22 (2007).
- 1026 52. The Gene Ontology Consortium. Expansion of the Gene Ontology knowledgebase and  
1027 resources. *Nucleic Acids Res.* **45**, D331–D338 (2017).
- 1028 53. Jaccard, P. Distribution de la flore alpine dans le bassin des Dranses et dans quelques  
1029 régions voisines. *Bull. Soc. Vaud. sci. nat.* **37**, 241–272 (1901).
- 1030 54. Krzywinski, M., Birol, I., Jones, S. J. M. & Marra, M. A. Hive plots—rational approach to  
1031 visualizing networks. *Brief. Bioinform.* **13**, 627–644 (2012).
- 1032 55. Van Der Maaten, L. & Hinton, G. Visualizing High-Dimensional Data Using t-SNE. *J.*  
1033 *Mach. Learn. Res.* **9**, 26 (2008).
- 1034 56. Van Der Maaten, L. Accelerating t-SNE using tree-based algorithms. *J. Mach. Learn.*  
1035 *Res.* **15**, 3221–3245 (2014).
- 1036 57. García-Aguilar, A. & Cuezva, J. M. A Review of the Inhibition of the Mitochondrial ATP  
1037 Synthase by IF1 in vivo: Reprogramming Energy Metabolism and Inducing  
1038 Mitohormesis. *Front. Physiol.* **9**, 1322 (2018).
- 1039 58. Orchard, S. *et al.* The MIntAct project—IntAct as a common curation platform for 11  
1040 molecular interaction databases. *Nucleic Acids Res.* **42**, D358–63 (2014).
- 1041 59. Stark, C. *et al.* BioGRID: a general repository for interaction datasets. *Nucleic Acids*  
1042 *Res.* **34**, D535–9 (2006).
- 1043 60. Szklarczyk, D. *et al.* The STRING database in 2017: quality-controlled protein-protein  
1044 association networks, made broadly accessible. *Nucleic Acids Res.* **45**, D362–D368  
1045 (2017).
- 1046 61. The UniProt Consortium. UniProt: the universal protein knowledgebase. *Nucleic Acids*  
1047 *Res.* **45**, D158–D169 (2017).

- 1048 62. Forbes, S. A. *et al.* COSMIC: somatic cancer genetics at high-resolution. *Nucleic Acids*  
1049 *Res.* **45**, D777–D783 (2017).
- 1050 63. Piñero, J. *et al.* DisGeNET: a comprehensive platform integrating information on human  
1051 disease-associated genes and variants. *Nucleic Acids Res.* **45**, D833–D839 (2017).
- 1052 64. Andrews, S. J. & Rothnagel, J. A. Emerging evidence for functional peptides encoded  
1053 by short open reading frames. *Nat. Rev. Genet.* **15**, 193–204 (2014).
- 1054 65. Aspden, J. L. *et al.* Extensive translation of small Open Reading Frames revealed by  
1055 Poly-Ribo-Seq. *Elife* **3**, e03528 (2014).
- 1056 66. D’Lima, N. G. *et al.* A human microprotein that interacts with the mRNA decapping  
1057 complex. *Nat. Chem. Biol.* **13**, 174–180 (2017).
- 1058 67. Chu, Q. *et al.* Identification of Microprotein-Protein Interactions via APEX Tagging.  
1059 *Biochemistry* (2017). doi:10.1021/acs.biochem.7b00265
- 1060 68. Slavoff, S. A. *et al.* Peptidomic discovery of short open reading frame-encoded peptides  
1061 in human cells. *Nat. Chem. Biol.* **9**, 59–64 (2013).
- 1062 69. Meyer, B., Wittig, I., Trifilieff, E., Karas, M. & Schagger, H. Identification of two proteins  
1063 associated with mammalian ATP synthase. *Mol. Cell. Proteomics* **6**, 1690–1699 (2007).
- 1064 70. Chen, R., Runswick, M. J., Carroll, J., Fearnley, I. M. & Walker, J. E. Association of two  
1065 proteolipids of unknown function with ATP synthase from bovine heart mitochondria.  
1066 *FEBS Lett.* **581**, 3145–3148 (2007).
- 1067 71. Fujikawa, M., Ohsakaya, S., Sugawara, K. & Yoshida, M. Population of ATP synthase  
1068 molecules in mitochondria is limited by available 6.8-kDa proteolipid protein (MLQ).  
1069 *Genes Cells* **19**, 153–160 (2014).
- 1070 72. Borner, G. H. H. *et al.* Multivariate proteomic profiling identifies novel accessory proteins  
1071 of coated vesicles. *J. Cell Biol.* **197**, 141–160 (2012).
- 1072 73. Signorile, A., Sgaramella, G., Bellomo, F. & De Rasmo, D. Prohibitins: A Critical Role in  
1073 Mitochondrial Functions and Implication in Diseases. *Cells* **8**, (2019).
- 1074 74. Brennan, R. *et al.* Investigating nucleo-cytoplasmic shuttling of the human DEAD-box  
1075 helicase DDX3. *Eur. J. Cell Biol.* **97**, 501–511 (2018).
- 1076 75. Szklarczyk, D. *et al.* STRING v11: protein-protein association networks with increased  
1077 coverage, supporting functional discovery in genome-wide experimental datasets.  
1078 *Nucleic Acids Res.* **47**, D607–D613 (2019).
- 1079 76. Schrader, M., Costello, J. L., Godinho, L. F., Azadi, A. S. & Islinger, M. Proliferation and  
1080 fission of peroxisomes - An update. *Biochim. Biophys. Acta* **1863**, 971–983 (2016).
- 1081 77. Schrader, M., Costello, J., Godinho, L. F. & Islinger, M. Peroxisome-mitochondria  
1082 interplay and disease. *J. Inherit. Metab. Dis.* **38**, 681–702 (2015).
- 1083 78. Devine, M. J., Birsa, N. & Kittler, J. T. Miro sculpts mitochondrial dynamics in neuronal  
1084 health and disease. *Neurobiol. Dis.* **90**, 27–34 (2016).
- 1085 79. Costello, J. L. *et al.* Predicting the targeting of tail-anchored proteins to subcellular  
1086 compartments in mammalian cells. *J. Cell Sci.* **130**, 1675–1687 (2017).
- 1087 80. Okumoto, K. *et al.* New splicing variants of mitochondrial Rho GTPase-1 (Miro1)  
1088 transport peroxisomes. *J. Cell Biol.* **217**, 619–633 (2018).
- 1089 81. Castro, I. G. *et al.* A role for Mitochondrial Rho GTPase 1 (MIRO1) in motility and  
1090 membrane dynamics of peroxisomes. *Traffic* **19**, 229–242 (2018).
- 1091 82. Rodríguez-Serrano, M., Romero-Puertas, M. C., Sanz-Fernández, M., Hu, J. &

- 1092 Sandalio, L. M. Peroxisomes Extend Peroxules in a Fast Response to Stress via a  
1093 Reactive Oxygen Species-Mediated Induction of the Peroxin PEX11a. *Plant Physiol.*  
1094 **171**, 1665–1674 (2016).
- 1095 83. Mattiazzi Ušaj, M. *et al.* Genome-Wide Localization Study of Yeast Pex11 Identifies  
1096 Peroxisome-Mitochondria Interactions through the ERMES Complex. *J. Mol. Biol.* **427**,  
1097 2072–2087 (2015).
- 1098 84. Shai, N. *et al.* Systematic mapping of contact sites reveals tethers and a function for the  
1099 peroxisome-mitochondria contact. *Nat. Commun.* **9**, 1761 (2018).
- 1100 85. Pickrell, J. K. *et al.* Understanding mechanisms underlying human gene expression  
1101 variation with RNA sequencing. *Nature* **464**, 768–772 (2010).
- 1102 86. Barrett, T. *et al.* NCBI GEO: archive for functional genomics data sets--update. *Nucleic*  
1103 *Acids Res.* **41**, D991–5 (2013).
- 1104 87. Szklarczyk, D. *et al.* STRING v10: protein-protein interaction networks, integrated over  
1105 the tree of life. *Nucleic Acids Res.* **43**, D447–52 (2015).
- 1106 88. Gandhi, S. J., Zenklusen, D., Lionnet, T. & Singer, R. H. Transcription of functionally  
1107 related constitutive genes is not coordinated. *Nat. Struct. Mol. Biol.* **18**, 27–34 (2011).
- 1108 89. Jovanovic, M. *et al.* Immunogenetics. Dynamic profiling of the protein life cycle in  
1109 response to pathogens. *Science* **347**, 1259038 (2015).
- 1110 90. R Core Team. R: A Language and Environment for Statistical Computing. (2018).
- 1111 91. Dowle, M. & Srinivasan, A. data.table: Extension of `data.frame`. (2018).
- 1112 92. Wickham, H. *ggplot2: Elegant Graphics for Data Analysis*. (Springer, 2016).
- 1113 93. Auguie, B. gridExtra: Miscellaneous Functions for 'Grid' Graphics. (2017).
- 1114 94. Wilke, C. O. cowplot: Streamlined Plot Theme and Plot Annotations for 'ggplot2'. (2018).
- 1115 95. Garnier, S. viridis: Default Color Maps from 'matplotlib'. (2018).
- 1116 96. Kustatscher, G., Wills, K. L. H., Furlan, C. & Rappsilber, J. Chromatin enrichment for  
1117 proteomics. *Nat. Protoc.* **9**, 2090–2099 (2014).
- 1118 97. Alabert, C. *et al.* Nascent chromatin capture proteomics determines chromatin dynamics  
1119 during DNA replication and identifies unknown fork components. *Nat. Cell Biol.* **16**,  
1120 281–293 (2014).
- 1121 98. Cox, J. & Mann, M. MaxQuant enables high peptide identification rates, individualized  
1122 p.p.b.-range mass accuracies and proteome-wide protein quantification. *Nat. Biotechnol.*  
1123 **26**, 1367–1372 (2008).
- 1124 99. Zhang, B. & Horvath, S. A general framework for weighted gene co-expression network  
1125 analysis. *Stat. Appl. Genet. Mol. Biol.* **4**, Article17 (2005).
- 1126 100. Langfelder, P. & Horvath, S. WGCNA: an R package for weighted correlation network  
1127 analysis. *BMC Bioinformatics* **9**, 559 (2008).
- 1128 101. Langfelder, P. & Horvath, S. Fast R Functions for Robust Correlations and Hierarchical  
1129 Clustering. *J. Stat. Softw.* **46**, (2012).
- 1130 102. Sing, T., Sander, O., Beerenwinkel, N. & Lengauer, T. ROCR: visualizing classifier  
1131 performance in R. *Bioinformatics* **21**, 3940–3941 (2005).
- 1132 103. Krijthe, J. H. Rtsne: T-Distributed Stochastic Neighbor Embedding using Barnes-Hut  
1133 Implementation. URL: <https://github.com/jkrijthe/Rtsne> (2015).
- 1134 104. Csardi, G. & Nepusz, T. The igraph software package for complex network research.  
1135 *InterJournal*, 1695 (2006).

- 1136 105.Schloerke, B. *et al.* GGally: Extension to 'ggplot2'. (2018).  
1137 106.Butts, C. T. sna: Tools for Social Network Analysis. (2016).  
1138 107.Alexa, A. & Rahnenfuhrer, J. topGO: enrichment analysis for gene ontology. *R package*  
1139 *version 2.30.0* (2016).  
1140 108.Binns, D. *et al.* QuickGO: a web-based tool for Gene Ontology searching. *Bioinformatics*  
1141 **25**, 3045–3046 (2009).  
1142 109.Costello, J. L. *et al.* ACBD5 and VAPB mediate membrane associations between  
1143 peroxisomes and the ER. *J. Cell Biol.* **216**, 331–342 (2017).